https://doi.org/10.5194/egusphere-2025-5879
Preprint. Discussion started: 5 December 2025

Drivers of diurnal and seasonal dynamics of triple oxygen isotopes in atmospheric water vapor and precipitation at a Mediterranean forest site

Claudia Voigt[1,a], Christine Vallet-Coulomb[1], Clément Piel[2], Joana Sauze[2], Ilja M. Reiter[3], Jean-Philippe Orts[4], Françoise Chalié[1], Christophe Cassou[5], Irène Xueref-Remy[4], Anne Alexandre[1]

[1]Aix-Marseille University, CNRS, IRD, INRAE, CEREGE, 13545 Aix-en-Provence, France
[2]ECOTRON Européen de Montpellier, UAR 3248, Montpellier University, CNRS, 34980 Montferrier-sur-Lez, France
[3]Research Federation ECCOREV, FR3098, CNRS, 13545 Aix-en-Provence, France
[4]IMBE, CNRS, University of Avignon, Aix-Marseille University, IRD, 13397 Marseille, France
[5]CECI, Université de Toulouse, Cerfacs, CNRS, Toulouse, France
[a]present address: Institute of Soil Sciences and Site Ecology, TU Dresden, 01737 Tharandt, Germany

Correspondence to: Claudia Voigt (claudia.voigt@tu-dresden.de)

Abstract.

Triple oxygen isotopes are a powerful tracer of hydrological processes, yet their variability in atmospheric water vapor and the processes driving them remain poorly understood. We present a one-year record of triple oxygen and hydrogen isotopes of atmospheric water vapor (V) measured at four heights below and above a downy oak forest canopy at the AnaEE platform O_3HP in the French Mediterranean. This vapor dataset is complemented by isotope data from rainfall and groundwater, as well as monthly measurements of stomatal conductance and transpiration. Our results demonstrate that $^{17}O\text{-excess}_V$ is principally driven by evaporation processes. Seasonal variations in $^{17}O\text{-excess}_V$ ranging from 33 ± 9 per meg in winter to 25 ± 6 per meg in summer, reflect evaporative conditions in oceanic moisture sources. Diurnal variations, particularly pronounced in summer, with daytime maxima around 33 ± 6 per meg and nighttime minima around 16 ± 7 per meg, are linked to local evapotranspiration and isotope exchange between leaf waters and the atmosphere. On a monthly scale, precipitation is generally close to isotope equilibrium with atmospheric water vapor, except in summer when rain re-evaporation occurs. At event scale, large deviations from isotope equilibrium can occur due to raindrop evaporation and incomplete re-equilibration. Our findings enhance the mechanistic basis for interpreting precipitation isotopes in paleoclimate context, improves the robustness of isotope-based model evaluation, and highlights the potential of ^{17}O-excess for better understanding of land-atmosphere water exchange across diverse climate and vegetation contexts.

1 Introduction

The analysis of triple oxygen isotopes (^{16}O, ^{17}O, ^{18}O) has become an important tool in the study of the hydrological cycle. The secondarily derived ^{17}O-excess parameter [$= \ln(\delta^{17}O + 1) - 0.528 \ln(\delta^{18}O + 1)$] complements the traditional d-excess

https://doi.org/10.5194/egusphere-2025-5879
Preprint. Discussion started: 5 December 2025

[= $\delta^2H - 8\ \delta^{18}O$] in the assessment of hydrological processes. In contrast to d-excess, ^{17}O-excess is only weakly affected by temperature (Barkan & Luz, 2005) and, therefore, insignificantly influenced by condensation and Rayleigh distillation during rainout (Landais et al., 2008). Hence, variations of ^{17}O-excess are mainly driven by diffusive fractionation processes that make it a valuable tracer for climate conditions during evaporation, mainly atmospheric relative humidity (RH) (Alexandre et al., 2018, 2019; Gázquez et al., 2018, 2023; Outrequin et al., 2021; Surma et al., 2015, 2018). Moreover, the ^{17}O-excess of surface waters can be used for identifying recharge conditions during lake evaporation (Surma et al., 2015, 2018) and mixing processes between evaporated and unevaporated waters (Voigt et al., 2021), lake hydrological balancing (Pierchala et al., 2021; Voigt et al., 2024) and water exchange at the soil-plant-atmosphere interface (Landais et al., 2006; Li et al., 2017; Voigt et al., 2023). It is also useful for improving quantifications of biogeochemical fluxes (O_2, CO_2 Koren et al., 2019). However, little is known about the variability of ^{17}O-excess in atmospheric water vapor and the processes driving it.

Comprehensive knowledge of these processes is essential for constraining the water cycle at the soil-plant-atmosphere interface and for iso-hydrological modeling of evaporation processes. So far, measurements of ^{17}O-excess in atmospheric water vapor have been restricted to discrete samples collected by cryogenic distillation and limited to a handful of studies. Data from atmospheric water vapor above the Southern Ocean (Uemura et al., 2010), continental atmospheric water vapor above northern Greenland (Landais et al., 2012) and a tropical island (Uechi and Uemura, 2019) suggest the potential of ^{17}O-excess to trace changes in relative humidity at the oceanic moisture sources. However, mixing of air masses from different sources, terrestrial moisture recycling, raindrop re-evaporation and local sublimation can alter ^{17}O-excess of continental atmospheric water vapor and associated precipitation (Arellano et al., 2024; Aron et al., 2021; Giménez et al., 2021; S. He et al., 2021; Landais et al., 2010, 2012; Liang et al., 2024; Ranjan et al., 2021; Surma et al., 2021; Voarintsoa, 2025; Zhang et al., 2025). The respective impact of these processes, inherent to the water cycle, on the ^{17}O-excess and d-excess of precipitation has been recently theorized by Xia et al. (2023). Furthermore, under certain conditions, stratospheric intrusions can increase the ^{17}O-excess of atmospheric water vapor to more than 100 per meg (Lin et al., 2013).

Here, we used a cavity ring-down spectrometer (CRDS) to continuously measure $\delta^{17}O$, $\delta^{18}O$ and δ^2H in atmospheric water vapor at multiple heights – below, within and above a deciduous Mediterranean oak forest canopy – over the course of one year. Additionally, we analyzed the triple oxygen and hydrogen isotope composition of precipitation samples collected at quasi-event scale. Meteorological parameters and vegetation phenology, stomatal conductance and transpiration were monitored throughout the oak forest's growing season (live foliage). We identified oceanic moisture sources and conditions during evaporation from the ocean that formed the observed air masses and categorized them into eight synoptic patterns spread over the year. Furthermore, we determine the key processes that control the variability in the triple oxygen isotopic composition of atmospheric water vapor on seasonal, monthly and daily scales. We also examined the hypothesis of isotope equilibrium between atmospheric water vapor and precipitation, which is often used in surface iso-hydrological models (e.g., Arnault et al., 2021).

https://doi.org/10.5194/egusphere-2025-5879
Preprint. Discussion started: 5 December 2025

2 Materials and Methods

2.1 Study site, meteorological and vegetation measurements

The AnaEE *in natura* experimental platform O_3HP is situated in a Mediterranean forest about 70 km north of Marseille (France) at an altitude of 680 m above sea level (43.935° N, 5.711° E). The forest is dominated by downy oak (*Quercus pubescens Willd.*) with co-dominant of Montpellier maple (*Acer monspessulanum L.*, 25% of canopy leaf mass). The tree canopy height is between 2 and 6 m and there is a low-density understory of grasses, forbs, and shrubs. In February 2021, a 5.5 m^2 plot of the C3 grass species *Festuca arundinacea* was set up in the understory of the forest for another experiment (Voigt et al., 2023).

The following climate parameters were measured on the experimental site: global solar radiation at 6 m above ground (LI-200, LI-COR Biosciences Inc., Nebraska, USA), precipitation amount (15189 H, LAMBRECHT meteo GmbH, Göttingen, Germany), RH and atmospheric temperature (T_{air}) at 0.6 m height next to the grass plot and at 1.5 m, 1.9 m, 4.4 m and 6.15 m height in the oak forest canopy (HMP155, Vaisala Oyj, Vantaa, Finland). Furthermore, we used RH, T_{air}, wind speed and direction, and atmospheric pressure measured at 10 m height on the on-site ICOS Tower. Each parameter was extracted in hourly resolution from the COOPERATE database (Reiter et al., 2015).

Pictures of the forest canopy were taken every day from a fixed point to provide information on the oak phenology. Stomatal conductance (g_s) and transpiration were continuously measured on a single oak leaf in the sun-crown of the canopy using a Li-6400 XT gas exchange system (LI-COR Biosciences Inc., Nebraska, USA) over 24 hours in the early, middle and last stage of the oak growing season (on June 22-23, August 27-28 and October 22-23, respectively). Simultaneously, the spatial variability of g_s, was assessed by hourly g_s measurements on the abaxial side of 18 oak leaves in the shade- and sun-crown of six different trees (i.e. 3 leaves per tree), using an AP4 porometer (Delta-T Devices LTD, Cambridge, UK).

2.2 Isotope monitoring of groundwater, precipitation and atmospheric water vapor

All isotope data presented herein are expressed in delta-notation and normalized on the Vienna Standard Mean Ocean Water – Standard Light Antarctic Precipitation (VSMOW-SLAP) scale. The secondary isotope parameters d-excess and ^{17}O-excess are derived from primary isotope values as following:

$$\text{d-excess} = \delta\,^{2}\text{H} - 8\delta^{18}\text{O} \quad (1)$$

$$^{17}\text{O-excess} = \delta'^{17}\text{O} - 0.528\delta'^{18}\text{O} \quad (2)$$

with $\delta' = \ln(\delta + 1)$. Throughout this study, δ-values and d-excess are reported in per mil (10^{-3}, ‰, parts per thousand), while ^{17}O-excess is reported in per meg (i.e., 0.001‰).

The inlets of four 1/4-inch wide PFA tubes (PFA-T4-062-100, Swagelok, Ohio, US) were positioned at 0.4 m above a grass plot that was set up for another experiment, and at 1.5 m, 3.5 m, and 12.5 m above ground level (agl) – below, within and above the downy oak forest canopy, respectively. The tubing was insulated and heated to 40–50°C using self-regulating heat wire to prevent condensation and continuously pumped at a flow rate of ~5 L min^{-1} using oil-free diaphragm pumps. A funnel

https://doi.org/10.5194/egusphere-2025-5879
Preprint. Discussion started: 5 December 2025

covered by a net was placed at each inlet for protection from rain and suction of insects and large aerosol particles. A split of each line was passed to a 16-Port Distribution Manifold (A0311; Picarro Inc., California, USA) coupled to a cavity ring-down spectrometer (CRDS L2140-i; Picarro Inc., California, USA) installed in an air-conditioned building on the experimental site and operated in ^{17}O Dual Liquid/Vapor mode. The instrument subsampled the air from a selected tube with a flow rate lower than 0.4 mL min^{-1} for 70 minutes before switching to the next line. From January to May 2021, measurements were alternated only between tubes at 0.4 m above the grass plot and 12.5 m above the forest canopy, resulting in 9–10 measurements per height and day. From June to December 2021, measurements were alternated between all four heights, resulting in 4–5 measurements per height and day.

The calibration protocol of atmospheric water vapor isotope data is described in detail in Voigt et al. (2023). In brief, three liquid water standards that covered the expected isotope range of atmospheric water vapor at the study site were analyzed at a water mixing ratio of 11000 ppmv using an autosampler system (A0325, Picarro Inc., California, USA) coupled to a high-precision vaporizer (A0211, Picarro Inc., California, USA). The liquid standards were injected in a dry air stream, produced by a lubricated mobile air compressor (MONTECARLO FC2, ABAC air compressors, Italy), further dried using two drierite columns combined with a dry ice trap. Raw isotope compositions of the liquid standards of four consecutive measurement runs were averaged and then corrected to the water mixing ratio of the measured atmospheric water vapor, using the mean of three mixing ratio dependency functions that were determined on site for water mixing ratios between 3000 and 30000 ppmv in May 2021, October 2021 and January 2022 (see Fig. A1 in appendix of Voigt et al., 2023). The standards with the lowest and the highest isotope values were used for two-point calibration on VSMOW-SLAP scale, while the third standard with an isotope composition between the other two served as quality control. The precision of calibrated and integrated atmospheric water vapor data was determined using a Monte Carlo simulation. Precision was better than ± 0.1 ‰, ± 0.2 ‰, ± 1.8 ‰ and ± 14 per meg, and ± 0.9 ‰ for $\delta^{17}O$, $\delta^{18}O$, $\delta^{2}H$, ^{17}O-excess, and d-excess, respectively.

Precipitation was collected in an evaporation-free rainfall collector (Rain Sampler 1, Palmex d.o.o., Zagreb, Croatia; Gröning et al., 2012), sampled monthly from June 2019 to December 2020 and on an event-based interval in 2021. The latter resulted in two snow and 53 rain samples. In addition, an on-site well, an underground spring, two springs in the village Saint-Michel-l'Observatoire and the nearby river Largue were sampled seasonally between May 2020 and October 2021 to constrain the isotope composition of groundwater. The triple oxygen and hydrogen isotope composition of precipitation, river, well and spring samples was determined using a second Picarro L2140-i CRDS, operated in ^{17}O-High Precision mode at CEREGE (Aix-en-Provence, France). The measurement protocol was described in detail previously (Vallet-Coulomb et al., 2021). The external reproducibility of a quality control standard (1 SD, n = 10) measured along with the samples in each sequence was ± 0.02‰, ± 0.04‰, ± 0.3‰ and ± 5 per meg, and ± 0.1‰ for $\delta^{17}O$, $\delta^{18}O$, $\delta^{2}H$, ^{17}O-excess, and d-excess, respectively.

To evaluate the significance of monthly variability in the isotope compositions of precipitation and atmospheric water vapor, we performed pairwise comparisons using Student's t-test and applied a Bonferroni correction (Bland and Altman, 1995). For each pair of months, we compared the average isotope composition (δ-values) with their standard deviations to determine statistically significant differences.

https://doi.org/10.5194/egusphere-2025-5879
Preprint. Discussion started: 5 December 2025

2.3 Assessment of isotope (dis)equilibrium between atmospheric water vapor and precipitation

The isotope composition of water vapor in isotope equilibrium with precipitation (hereafter equilibrium water vapor) is estimated from:

$$R_{Veq} = \frac{R_P}{\alpha_{eq,l\text{-}v}} \quad (3)$$

where RVeq is the isotope ratio in water vapor in equilibrium with precipitation, R_P is the measured isotope ratio in precipitation and $\alpha_{eq,l-v}$ is the liquid-vapor equilibrium isotope fractionation factor. We used temperature-dependent equilibrium fractionation factors for $^2H^1HO/^1H_2O$ and $^1H_2{}^{18}O/^1H_2{}^{16}O$ from Majoube (1971). The equilibrium fractionation factor for $^1H_2{}^{17}O/^1H_2{}^{16}O$ was derived from $^{17}\alpha_{eq,l-v} = {}^{18}\alpha_{eq,l-v}{}^{0.529}$ (Barkan & Luz, 2005). We used T_{air} measured on the ICOS tower at 10 m agl. Note that using different air temperatures measured between 0.4–100 m agl does not significantly influence the results.

Like Graf et al. (2019), we denote the differences between equilibrium water vapor and water vapor measured at 12.5 m agl as:

$$\Delta\delta^{18}O_{Veq\text{-}V} = \delta^{18}O_{Veq} - \delta^{18}O_V \quad (4)$$

$$\Delta\text{d-excess}_{Veq\text{-}V} = \text{d-excess}_{Veq} - \text{d-excess}_V \quad (5)$$

$$\Delta^{17}\text{O-excess}_{Veq\text{-}V} = {}^{17}\text{O-excess}_{Veq} - {}^{17}\text{O-excess}_V \quad (6)$$

A negative value of $\Delta\delta^{18}O_{Veq\text{-}V}$ (Δd-excess$_{Veq\text{-}V}$, Δ^{17}O-excess$_{Veq\text{-}V}$) indicates that $\delta^{18}O$ (d-excess, ^{17}O-excess) of precipitation is lower than expected from isotope equilibrium with near-surface atmospheric water vapor. Inversely, positive values of $\Delta\delta^{18}O_{Veq\text{-}V}$ (Δd-excess$_{Veq\text{-}V}$, Δ^{17}O-excess$_{Veq\text{-}V}$) indicate that precipitation has higher $\delta^{18}O$ (d-excess, ^{17}O-excess) compared to the expected equilibrium value.

2.4 Weather regimes, air mass back trajectory analysis and oceanic moisture source identification

Synoptic atmospheric variability over Europe can be characterized using weather regimes (Cassou, 2008; Cassou et al., 2005; Michelangeli et al., 1995; Vautard, 1990). To determine the dominant weather regimes during the study period, large-scale atmospheric circulation fields for the North-Atlantic-European region (20ºN–80ºN and 80ºW–30ºE) were obtained from the European Centre for the Medium-Range Weather Forecasts (ECMWF) ERA5 reanalysis data and classified over 1989–2022. The classification was based on daily-averaged 500 hPa geopotential height (Z500) fields, interpolated onto a 2.5º x 2.5º grid and clustered using the k-means algorithm (Hersbach et al., 2020). Each day was assigned to a specific weather regime based on the criterion of minimum Euclidian distance.

To identify oceanic moisture sources of the local atmospheric water vapor qualitatively, backward trajectory analysis was performed using the Hybrid Single Particle Lagrangian Integrated Trajectory model (HYSPLIT) (Stein et al., 2015). Meteorological input data were obtained from the Global Data Assimilation System (GDAS) dataset at a spatial resolution of 0.25º x 0.25º. As most of the atmospheric moisture resides in the lowermost 2000 m agl (Bershaw et al., 2012), back-trajectories

https://doi.org/10.5194/egusphere-2025-5879
Preprint. Discussion started: 5 December 2025

were initiated at 1500 m agl. Note that back-trajectories initiated at 500 m and 3000 m showed similar paths. Trajectories were computed hourly throughout 2021 extending 168 hours (7 days) backward. This resulted in a total of 8760 trajectories covering 365 measurement days.

Back-trajectories were classified into five regions: (i) Mediterranean, (ii) East Atlantic – Mediterranean, (iii) North Atlantic–Continental Europe, (iv) Continental Europe and (v) Northern Europe – Continental Europe. All trajectories that started above the East Atlantic also passed over the Mediterranean Sea. When starting above the North Atlantic or Northern Europe, the trajectories also passed over Continental Europe. In addition, back-trajectories that passed over more than one of these well-defined sources were classified as *multiple sources*. For precipitation samples, all air mass backward trajectories of hours when rain was detected on-site were compiled. A single source region was assigned to the event if more than 80 % of the rainfall come from that source. Otherwise, the source of precipitation was classified as originating from multiple source regions.

2.5 Climate conditions and isotope composition of the atmospheric water vapor at the oceanic moisture sources

Monthly averages of sea surface temperature (SST), T_{air} and dew point temperature at 2 m above the ocean surface (T_{dew}) were obtained from ERA5 hourly data for the region spanning 20º-70ºN latitude and -50º-40ºE longitude (Hersbach et al., 2020). RH over the ocean was derived from T_{air} and T_{dew} and subsequently normalized to SST (RH_{SST}).

The triple oxygen and hydrogen isotope composition of water vapor evaporated from the ocean was estimated using a simple evaporation model (Craig & Gordon, 1965), assuming that all water vapor above the ocean is derived from local evaporation (i.e. the closure assumption; Merlivat & Jouzel, 1979). Seawater $\delta^{18}O$ and d-excess values were taken from the CISE-LOCEAN seawater isotopic database (waterisotopes-CISE-LOCEAN, 2025) and range from 0.3 to 1.3‰ and -0.9 to -2.3‰, respectively. For ^{17}O-excess of seawater, the global average value of -5 per meg from the only existing compilation is used (Luz & Barkan, 2010). Further, we used a turbulence coefficient of 0.33, which is within the range of previously reported values for open-ocean evaporation (see, e.g., Gat, 1996; Pfahl & Wernli, 2008; Uemura et al., 2010).

3 Results

3.1 Variability of local meteorological parameters, phenology, stomatal conductance and transpiration

In 2021, annual average T_{air} and RH at O_3HP were 12 ºC and 63 %, respectively. The annual precipitation was 730 mm, which is about 150 mm lower than the average annual precipitation from 2008-2020 (Reiter et al., 2015). As typical for a Mediterranean climate, more than 70 % of precipitation occurred from April to May and between September and December, while summer months were the driest (Fig. 1a). The monthly atmospheric water mixing ratio (q) ranged from 7 mmol mol^{-1} in winter to 22 mmol mol^{-1} in summer. Despite the increase in q in summer, the lowest monthly RH was recorded in August (53 %), while the highest was observed in February (75 %), due to higher monthly T_{air} in summer (JJA, 21ºC) than in winter (DJF; 6ºC). The maximum planetary boundary layer height increased from 600 m agl in December to 1700 m agl in July. The average wind speed at 10 m height was 2.6 ± 0.3 m s^{-1} in 2021. One to eight windy days (daily average wind speed > 4 m s^{-1}; Obermann

https://doi.org/10.5194/egusphere-2025-5879
Preprint. Discussion started: 5 December 2025

et al., 2018) were observed per month. Windy days are mostly indicative for Mistral conditions – a strong northerly wind typical of the Provence region – and occurred most frequently in winter and spring.

In 2021, the average monthly q was 2 to 6 mmol mol^{-1} higher during the day than at night. T_{air} was 6 to 16ºC higher during the day, while RH increased by 26 to 50 % from day to night. The largest day-night differences occurred near the ground and in summer (Fig. A1-A3). During the day, q and T_{air} were highest near the ground, whereas RH was vertically homogenous (Fig. A1-A3). At night, the T_{air} vertical gradient was inverted, with the lowest values occurring near the ground, while q showed no vertical variation, resulting in decreasing RH from the surface to 10 m agl (Fig. A1-A3).

The first oak buds appeared in mid-April 2021. The oak leaves matured in May and senesced in November. Their stomatal conductance and transpiration followed the diurnal cycle of global solar radiation and RH (Fig. A4). During the three separate days of continuous measurement, daytime stomatal conductance and transpiration ranged from 20–60 mmol mol^{-1} and 0.5–1.8 mmol mol^{-1}, respectively. During the night, transpiration and stomatal conductance were always lower than 20 mmol mol^{-1} and 0.1 mmol mol^{-1}, respectively. Transpiration was highest at the beginning of the growing season in June, and the lowest in August, mainly determined by lower stomatal conductance, although the vapor pressure deficit had increased.

https://doi.org/10.5194/egusphere-2025-5879
Preprint. Discussion started: 5 December 2025

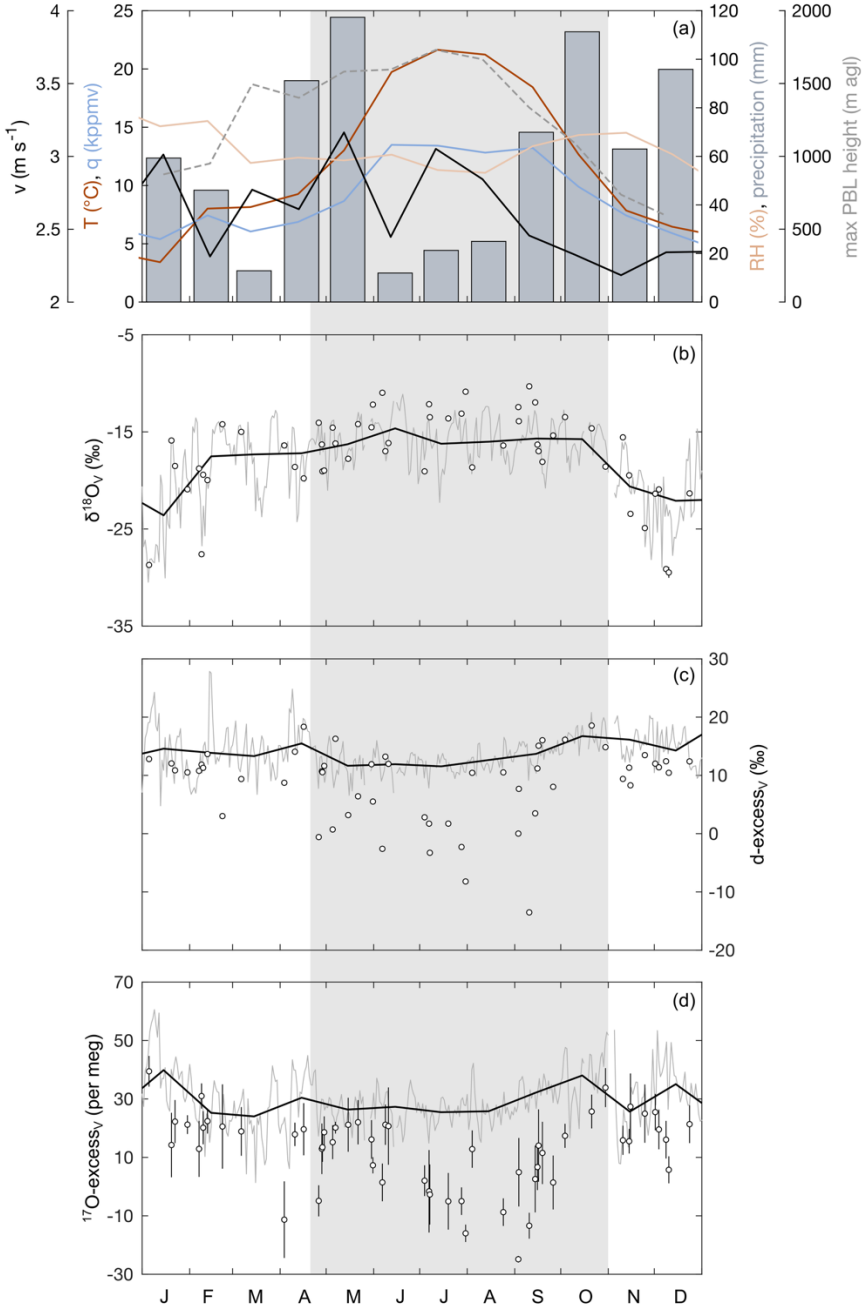

Figure 1: Time series of meteorological data and the isotope composition of atmospheric water vapor measured at 12.5 m agl and estimated from isotope equilibrium with precipitation in 2021. (a) Monthly precipitation amount and monthly average temperature (T_{air}), atmospheric water mixing ratio (q), wind speed (v), and relative humidity (RH) measured at 10 m agl. The grey dashed line shows the monthly average maximum planetary boundary layer height for the 0.25°×0.25° grid field covering the study site (Guo et al., 2022). (b)-(d) Solid lines represent daily (grey) and monthly (black) average isotope composition of atmospheric water vapor measured at 12.5 m agl. Circles show the isotope composition of water vapor estimated from isotope equilibrium with event-based precipitation samples using T_{air} observed at 10 m agl. The grey shaded area marks the oak forest growing season.

https://doi.org/10.5194/egusphere-2025-5879
Preprint. Discussion started: 5 December 2025

3.2 Isotope composition of precipitation and groundwater

The annual amount-weighted average isotope values of precipitation in 2021 were -7.5 ± 2.3 ‰ for $\delta^{18}O_P$, -48.1 ± 20.2 ‰ for δ^2H_P, 11.6 ± 3.5 ‰ for d-excess$_P$ and 27 ± 9 per meg for ^{17}O-excess$_P$ (Fig. 2). These values are close to those obtained for 2020 and indistinguishable from those obtained for the whole precipitation dataset from June 2019 to December 2021 (Table B1). The springs, the well and the river Largue sampled seasonally between December 2020 and October 2021 showed little spatial and seasonal variability (Table B1) and averaged to -7.3 ± 0.5 ‰ for $\delta^{18}O$, -47.0 ± 3.6 ‰ for δ^2H, 11.2 ± 0.6 ‰ for d-excess and 29 ± 5 per meg for ^{17}O-excess. These values coincide with the annual amount-weighted average isotope composition of precipitation.

Monthly amount-weighted average isotope values of precipitation varied between -11.8 and -1.1 ‰ for $\delta^{18}O_P$, between -78.8 and -6.5 ‰ for δ^2H_P, between -1.4 and 18.2 ‰ for d-excess$_P$ and between 1 and 41 per meg for ^{17}O-excess$_P$ (Table B1). In general, monthly values of $\delta^{18}O_P$ and δ^2H_P were low in winter and varied in their upper range from spring to autumn. Inversely, monthly values of d-excess$_P$ and ^{17}O-excess$_P$ were low in summer and tended to higher values in autumn and winter.

The isotope values of event-based rain samples ranged from -18.4 to -0.2 ‰ for $\delta^{18}O_P$, from -142.5 to -7.8 ‰ for δ^2H_P, from -13.0 to 20.5 ‰ for d-excess$_P$ and from -15 to 51 per meg for ^{17}O-excess$_P$ (Table S1). The two snow samples had the lowest $\delta^{18}O_P$ (-22 and -18 ‰, respectively) and δ^2H_P (-162 and -142‰, respectively) of the whole data set, while d-excess$_P$ (15.6 and 4.0 ‰) and ^{17}O-excess$_P$ (68 and 17 per meg) were variable. The seasonal variability of ^{17}O-excess$_P$ was generally higher than its variability from one event to another. In contrast, variability of $\delta^{18}O_P$ and d-excess$_P$ was often higher on event-scale than on seasonal scale (Student's t-test).

Linear regression through monthly amount-weighted average precipitation data for 2020 and 2021 (n = 22) gives (Fig. 2):

$$\delta^2H = 7.9\ (\pm 0.4)\ \delta^{18}O + 9.7\ (\pm 2.7)$$

$$\delta'^{17}O = 0.5263\ (\pm 0.0009)\ \delta'^{18}O + 0.0128\ (\pm 0.0064)$$

In the δ^2H-$\delta^{18}O$ system, the slope of the regression line is indistinguishable from that for Avignon (IAEA/WMO, 2025), located 70 km to the west of our study site (Fig. 2). It is close to that of the GMWL (8; Rozanski et al., 1993), but higher than the range of previously reported values for the western Mediterranean area (7.15-7.56; Celle-Jeanton et al., 2001; Giménez et al., 2021; Saighi, 2005). In the $\delta'^{17}O$-$\delta'^{18}O$ system, the slope of the regression line is lower than that of the GMWL (0.528; Luz & Barkan, 2010; Terzer-Wassmuth et al., 2023) but similar to the value obtained for temperate and intertropical areas (0.5265 Sharp et al., 2018; Terzer-Wassmuth et al., 2023). Notably, the slope of the regression line varies strongly from a year to another for both the δ^2H-$\delta^{18}O$ system (7.3-8.5) and the $\delta'^{17}O$-$\delta'^{18}O$ system (0.5254-0.5271). A longer precipitation isotope record is required to establish a robust local meteoric water line for the study site.

https://doi.org/10.5194/egusphere-2025-5879
Preprint. Discussion started: 5 December 2025

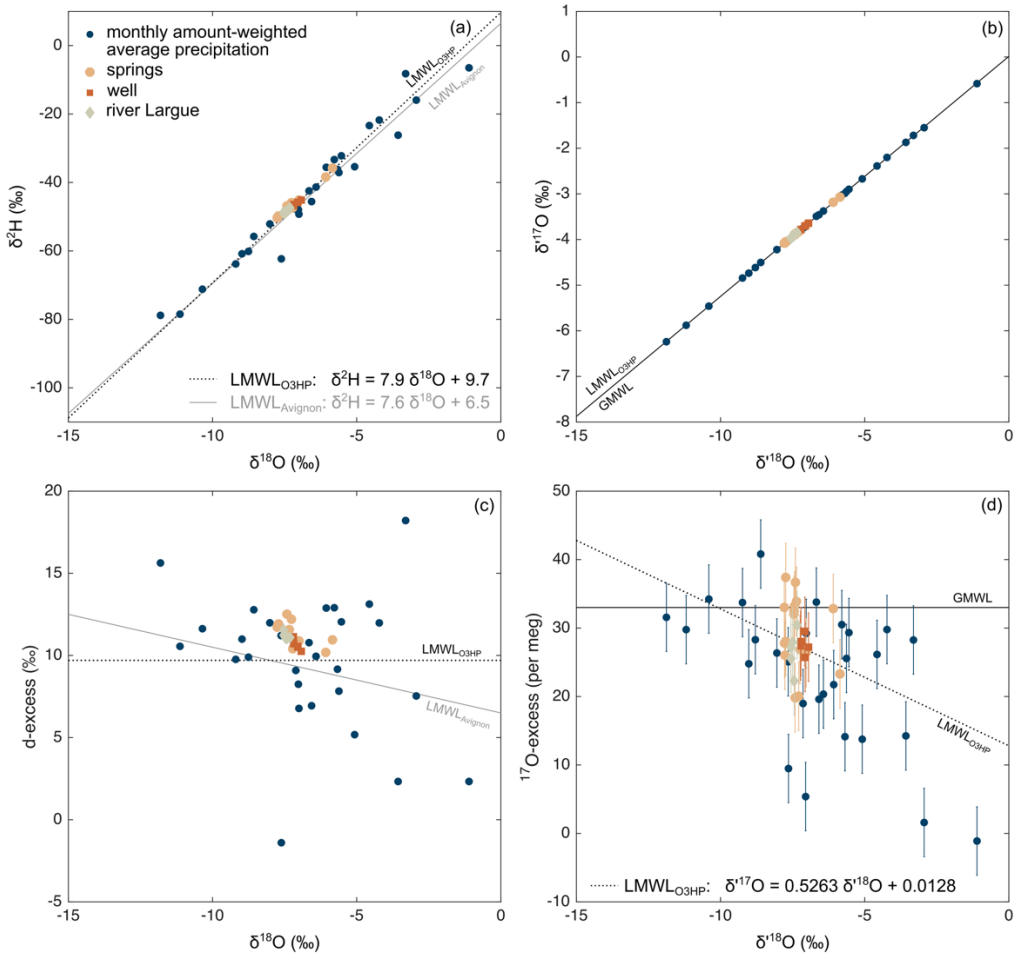

Figure 2: (a) δ^2H vs $\delta^{18}O$, (b) $\delta'^{17}O$ vs $\delta'^{18}O$, (c) d-excess vs $\delta^{18}O$ and (d) ^{17}O-excess vs $\delta'^{18}O$ of local meteoric waters collected in this study. Blue circles represent the monthly amount-weighted average isotope composition of precipitation collected at O_3HP between June 2019 and December 2021. Pale orange circles, orange squares and grey diamonds show the isotope composition of samples taken from springs, a well and the nearby river *Largue* in the surroundings of the study site (Table B1). The linear regression line through precipitation isotope data from 2020 and 2021 is indicated by the black dotted line. In addition, (a) and (c) show the local meteoric water line (LMWL) of Avignon for comparison (data derived from the global network of isotopes in precipitation (GNIP) database; IAEA/WMO, 2025). No ^{17}O-excess data was available for the Avignon dataset. Therefore, (b) and (d) show the global meteoric water line (GMWL) for comparison.

3.3 Isotope composition of atmospheric water vapor

The annual average isotope composition of atmospheric water vapor at 12.5 m agl was -17.7 ± 2.8 ‰ for $\delta^{18}O_V$, -128.1 ± 21.9 ‰ for δ^2H_V, 13.8 ± 1.7 ‰ for d-excess$_V$ and 30 ± 5 per meg for ^{17}O-excess$_V$, and indistinguishable from that measured at lower heights. Similar to precipitation, $\delta^{18}O_V$ and δ^2H_V were low in winter (-23.6 ‰ and -174.2 ‰, respectively) and high from spring to autumn, peaking in June (-14.6 ‰ and -105.2 ‰, respectively) (Table B2). Values of d-excess$_V$ were high in October and November (> 16 ‰) and low from May to July (< 12 ‰). In contrast, ^{17}O-excess$_V$ varied little throughout the

https://doi.org/10.5194/egusphere-2025-5879
Preprint. Discussion started: 5 December 2025

year (from 24 to 40 per meg). Low values (25-27 per meg) were recorded between May and August 2021, while highest values were observed in December (35 per meg) and January (40 per meg).

Day-to-day isotope variability of atmospheric water vapor was high (up to 9.3 ‰, 16.0 ‰ and 27 per meg for $\delta^{18}O_V$, d-excess$_V$ and ^{17}O-excess$_V$, respectively) and exceeded monthly and seasonal variability for d-excess$_V$ and ^{17}O-excess$_V$ (Fig. 1). There is no statistically significant difference in the daily average isotope composition of atmospheric water vapor on rainy and non-rainy days, indicating that precipitation had no significant influence on the isotope composition of atmospheric water vapor on daily and monthly scale.

Diurnal patterns of d-excess$_V$ and ^{17}O-excess$_V$ changed from a season to another (Fig. A6-A7). They can be illustrated by two examples (Fig. 3): In June, the month with the most active leaf gas exchange in the Mediterranean (Bartsch et al., 2020), d-excess$_V$ and ^{17}O-excess$_V$ were lowest at sunset and highest at noon, coinciding at noon with minimum RH, maximum transpiration and maximum q measured under the forest canopy. In December, a month characterized by the absence of alive tree foliage and transpiration and a thin planetary boundary layer, the amplitude of the diurnal cycle was three times lower than in June for the d-excess$_v$ and more than 15 times lower for the ^{17}O-excess$_V$. Diurnal isotope patterns were consistent for different heights, but the magnitude of variations decreased with distance from ground. Vertical isotope gradients were generally stronger during night, in line with limited atmospheric turbulent convection (Fig. A5).

https://doi.org/10.5194/egusphere-2025-5879
Preprint. Discussion started: 5 December 2025

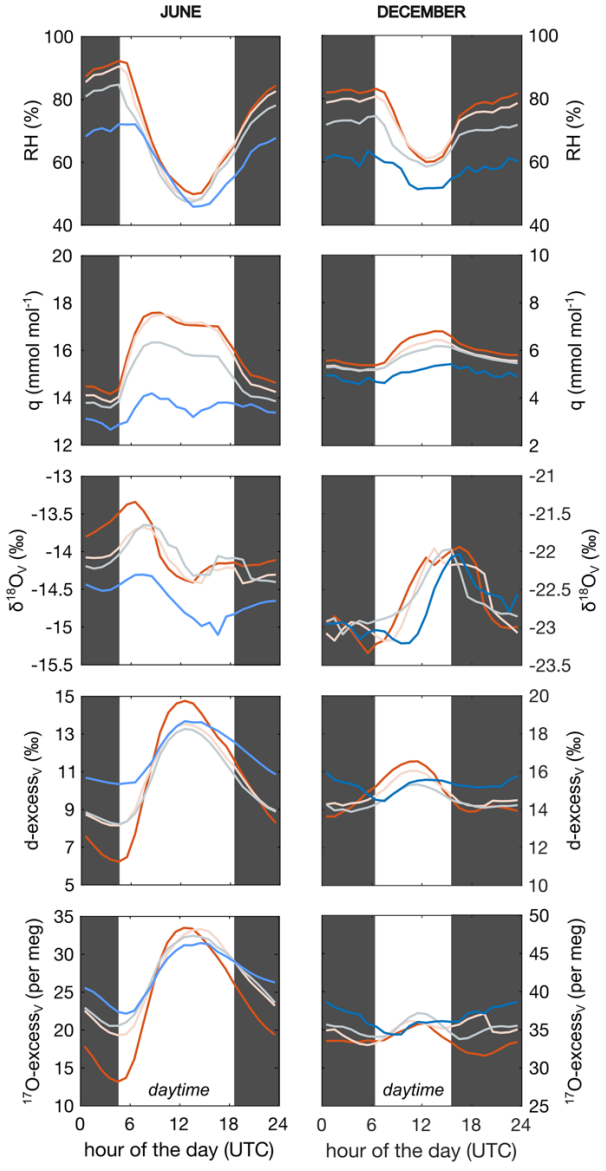

Figure 3: Monthly average daily cycle of relative humidity (RH), atmospheric water mixing ratio (q) and $\delta^{18}O_V$, d-excess$_V$ and ^{17}O-excess$_V$ of atmospheric water vapor at different measurements heights: above the grass plot (0.4 m agl; red), and below (1.5 m agl; pale), within (3.5 m agl; grey) and above (12.5 m agl, blue) the oak forest canopy. The left panels show monthly averages for June 2021, while the right panels show monthly averages for December 2021. For December, only the period from 01 to 25 December is included due to the lack of isotope data at 0.4 m, 1.5 m and 3.5 m after this date. Grey shaded areas represent night-time periods. Note that the vertical axes for June and December use similar scales but with different offsets.

3.4 Isotope (dis)equilibrium between precipitation and near-surface atmospheric water vapor

In winter, spring and late autumn, $\delta^{18}O_{Veq}$ was up to 5.5 ‰ lower than $\delta^{18}O_V$, while in summer $\delta^{18}O_{Veq}$ was up to 3.7 ‰ higher than $\delta^{18}O_V$. Values of d-excess$_{Veq}$ were generally close to d-excess$_V$ in winter, but up to 16 ‰ lower than d-excess$_V$ during the

https://doi.org/10.5194/egusphere-2025-5879
Preprint. Discussion started: 5 December 2025

oak growing season. Values of ^{17}O-excess$_{Veq}$ were slightly lower than ^{17}O-excess$_V$ in winter (~15 per meg) and up to 44 per meg lower during the oak growing season (Fig. 4).

However, on annual scale, $\delta^{18}O_V$ (-17.8 ± 2.8 ‰), δ^2H_V (-128.3 ± 21.9 ‰) and d-excess$_V$ (13.8 ± 1.7 ‰) were similar to their values expected from isotope equilibrium with precipitation (-17.8 ± 2.7 ‰, -130.1 ± 21.6 ‰ and 12.3 ± 3.1‰, respectively) due to their large variability from one event to another. In contrast, ^{17}O-excess$_V$ (30 ± 5 per meg) was in annual average 14 per meg higher than ^{17}O-excess$_{Veq}$ (16 ± 10 per meg).

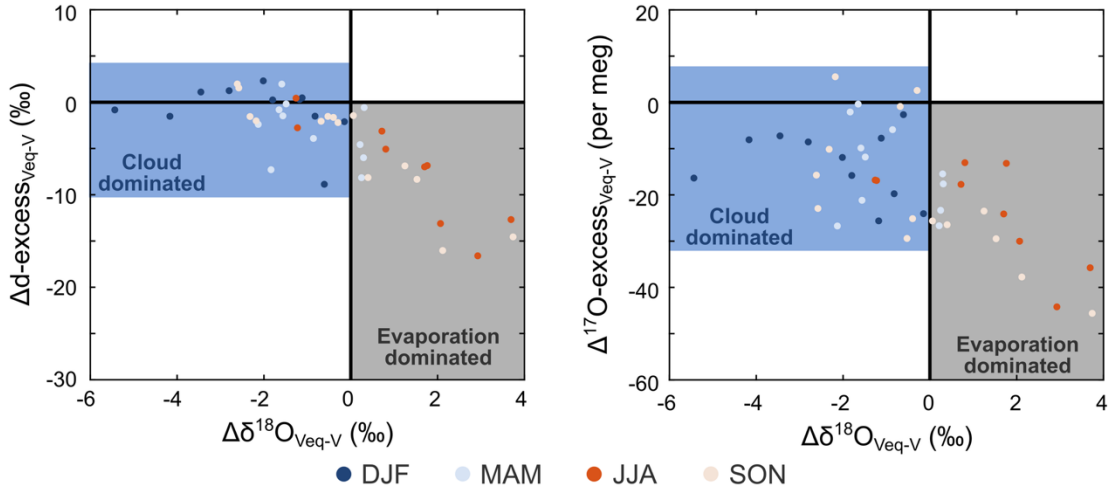

Figure 4: Isotope difference (Δ) between water vapor estimated from isotope equilibrium with precipitation (V_{eq}) and amount-weighted atmospheric water vapor measured at 12.5 m above ground level (V) for each precipitation event in 2021. Data is coloured according to season. Precipitation initially forms in isotope equilibrium with atmospheric water vapor at cloud height and re-equilibrates during descent as temperature and $\delta^{17}O$, $\delta^{18}O$ and δ^2H of atmospheric water vapor increase towards the surface (see Graf et al., 2019 for details). The blue-shaded area indicates samples for which the equilibration between precipitation and near-surface atmospheric water vapor is likely incomplete so that the cloud vapor signal still dominates the precipitation sample. Precipitation samples that correspond to data falling within the grey-shaded area are likely affected by re-evaporation during fall through the air column.

3.5 Relationships between meteorological parameters, phenology, stomatal conductance, transpiration and the isotope composition of atmospheric water vapor and precipitation

Monthly average $\delta^{18}O_V$ was strongly correlated with T_{air} and q (r^2 = 0.67 and 0.63, respectively). In contrast, d-excess$_V$ was only weakly correlated with these variables (r^2 = 0.26 and 0.29, respectively), and ^{17}O-excess$_V$ showed no significant relationship (Fig. A8). There is no correlation between the monthly average isotope composition of atmospheric water vapor and RH or wind speed.

Hourly means of $\delta^{18}O_V$, d-excess$_V$ and ^{17}O-excess$_V$ averaged by month (Fig. A6-A7) were strongly correlated with RH, T_{air} and transpiration during the oak forest growing season (r^2 > 0.55, > 0.73 and > 0.64, respectively). Correlations between ^{17}O-excess$_V$ and d-excess$_V$ were also strong during the oak forest growing season (r^2 = 0.52–0.93), peaking in June, while they were not correlated in winter.

https://doi.org/10.5194/egusphere-2025-5879
Preprint. Discussion started: 5 December 2025

For precipitation, monthly average $\delta^{18}O_P$ and d-excess$_P$ were weakly correlated with q, T_{air} and RH ($0.28 \leq r^2 \leq 0.38$), whereas ^{17}O-excess$_P$ showed stronger correlations with these variables ($0.44 \leq r^2 \leq 0.61$). No correlation was observed between the monthly average isotope composition of precipitation and precipitation amount.

At the event scale, $\delta^{18}O_P$ and ^{17}O-excess$_P$ remained weakly correlated with T_{air} ($r^2 = 0.41$ and 0.43, respectively) and q ($r^2 =$ 0.34 and 0.29, respectively), while d-excess$_P$ showed little or no correlation ($r^2 < 0.23$) (Fig. A9). Event-based isotope values of precipitation showed no correlation with RH or precipitation amount.

3.6 Relationships between moisture sources and the isotope composition of atmospheric water vapor and precipitation

For atmospheric water vapor, most of the moisture sources were either multiple (43% of the back-trajectories) or Continental Europe-North Atlantic (26%). For precipitation, most of the moisture sources were Mediterranean (42% of the back-trajectories) or East Atlantic-Mediterranean (24%) (Fig. A11).

The isotope compositions of water vapor and precipitation clustered by moisture sources were generally very similar (Fig. A11). However, air masses originating from the Mediterranean Sea and the East Atlantic-Mediterranean Sea had slightly higher $\delta^{18}O_V$ values (-15 to -17 ‰) than vapor coming from other sources (-18 to -20 ‰) (Fig. A11). Similarly, the amount-weighted $\delta^{18}O_P$ fed by Mediterranean (-6.5 ± 2.7 ‰) East Atlantic-Mediterranean (-7.9 ± 0.8 ‰) moisture sources was slightly higher than precipitation fed by North Atlantic-Continental Europe (-9.5 ± 2.6 ‰) moisture sources.

We also compared the monthly average isotope composition of atmospheric water vapor observed at O_3HP with those estimated above the four oceanic moisture sources (Fig. 5). The latter shows seasonal isotope variability which co-varies with sea surface temperature (SST) and RH normalized to sea surface temperature (RH_{SST}). Interestingly, RH_{SST} is not systematically lower above the Mediterranean Sea than above the Atlantic Ocean. For all sources, $\delta^{18}O_V$ is higher and d-excess$_V$ and ^{17}O-excess$_V$ are lower in summer than in winter. A similar seasonal trend is evident in the isotopic composition of the water vapor observed at O_3HP (Fig. 5). However, the $\delta^{18}O_V$ values at O_3HP were 3–11 ‰ lower than those estimated for the ocean sources. In contrast, the d-excess$_V$ at O_3HP was of the same order of magnitude as that of the ocean sources, while the observed ^{17}O-excess$_V$ was slightly higher (by 11 ± 5 per meg).

https://doi.org/10.5194/egusphere-2025-5879
Preprint. Discussion started: 5 December 2025

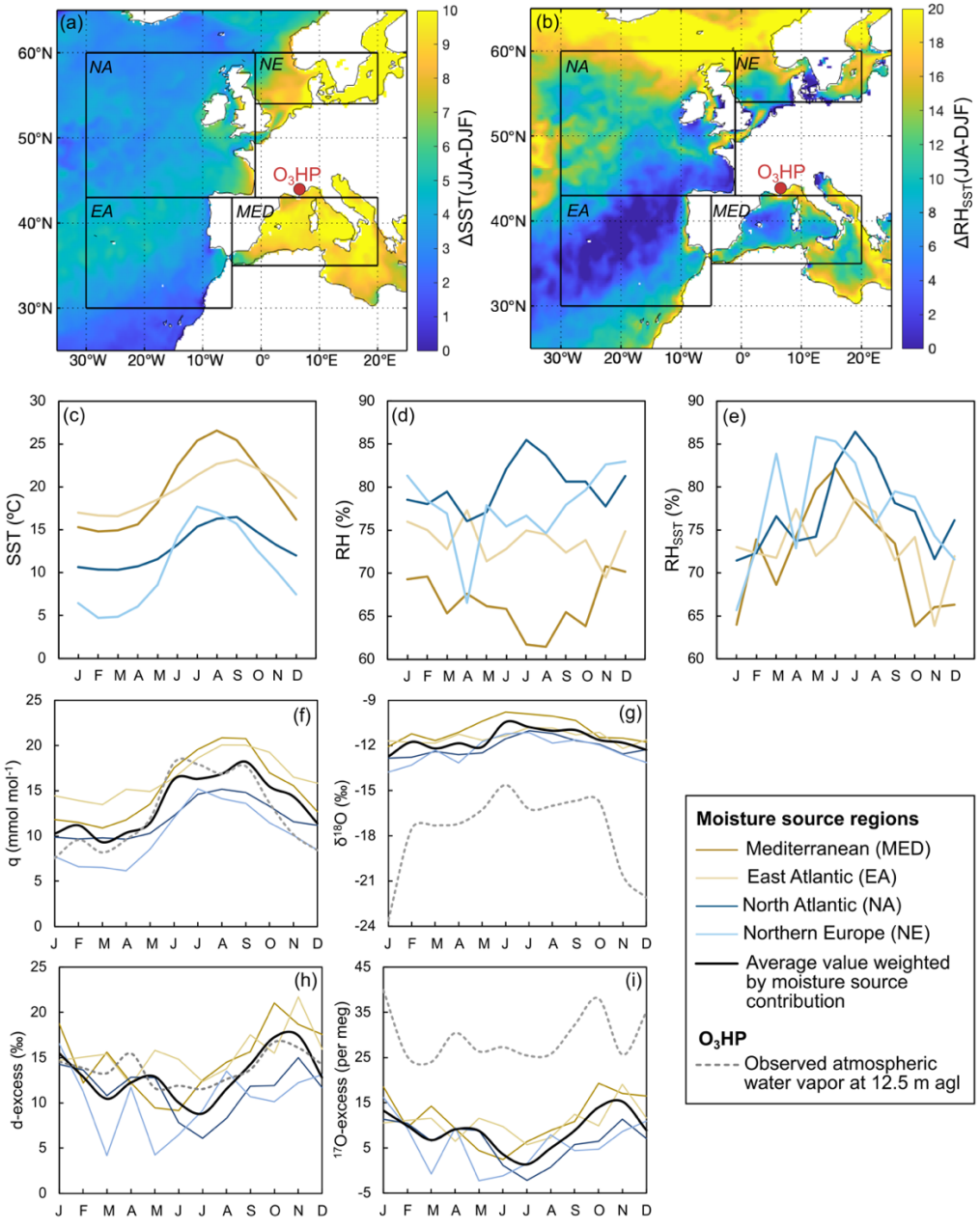

Figure 5: Seasonal and monthly variation in the isotope composition of atmospheric water vapor measured at O_3HP compared with climate parameters and isotope composition of atmospheric water vapor at the four main oceanic moisture sources. (a)-(b) Spatial variability of the difference between summer (JJA) and winter (DJF) sea surface temperature (SST) and relative humidity normalized to SST (RH_{SST}) in 2021. Data derived from ERA5 Reanalysis (Hersbach et al., 2020). The red circle indicates the location of the study site. (c)-(e) Monthly average SST, relative humidity above the ocean (RH) and RH_{SST} using ERA5 reanalysis dataset (Hersbach et al., 2020) for 2021. (f)-(i) Monthly average of atmospheric water mixing ratio (q), $\delta^{18}O_V$, d-$excess_V$ and ^{17}O-$excess_V$ measured at O_3HP at 12.5 m agl (dashed line) and estimated above the four oceanic moisture sources (solid lines). See Sect. 2.5 for more details on how the isotope composition of water vapor at each moisture source is estimated.

https://doi.org/10.5194/egusphere-2025-5879
Preprint. Discussion started: 5 December 2025

3.7 Relationship between weather regimes and the isotope compositions of atmospheric water vapor and precipitation

Four weather regimes were identified for 2021 in the North Atlantic area: the negative North Atlantic Oscillation (NAO^-), the positive North Atlantic Oscillation (NAO^+), the Blocking regime, and the Atlantic Ridge regime (Fig. A12). In winter, the Atlantic Ridge and NAO^- regimes were dominant, whereas NAO^+ occurred only sporadically. In summer (May–September), the Blocking/NAO+ regime was clearly the dominant, followed by NAO^-. Precipitation occurs most frequent during NAO^- phases (Fig. A13c, d). The isotopic compositions of water vapor and precipitation grouped by weather regime do not show significant differences, probably due to the combined influence of multiple moisture sources weakly isotopically contrasted as presented in section 3.6. It is also possible that the isotopic composition of water vapor measured at ground level differs slightly from that of the troposphere, which is directly linked to weather regimes (Tada et al., 2021).

4 Discussion

The isotope composition of atmospheric water vapor and precipitation is determined by the evaporation conditions at the oceanic moisture sources and is then modified by processes occurring during atmospheric transport and precipitation formation. These processes include progressive rainout during air mass transport, mixing of air masses from different sources, and the regional or local recycling of moisture through evapotranspiration. Locally, equilibration of raindrops with surrounding atmospheric water vapor and re-evaporation during falling can modify the isotope composition of precipitation. The isotopic effects of all these processes are physically well understood and have been modelled (Galewsky et al., 2016 and references therein; Xia et al., 2023). They are summarized in Figure 6. However, so far little is known about the combination of these effects on the triple isotopic composition of water vapor and precipitation as long-term triple oxygen isotope measurements of precipitation remain scarce, and no such datasets exist for atmospheric water vapor. The triple oxygen and hydrogen isotope dataset of atmospheric water vapor and precipitation gathered in the present study is used to evaluate the overall combined effect of these processes at different time scales. Further, the isotopic differences observed between the measured atmospheric water vapor and that estimated from isotope equilibrium with precipitation are discussed.

https://doi.org/10.5194/egusphere-2025-5879
Preprint. Discussion started: 5 December 2025

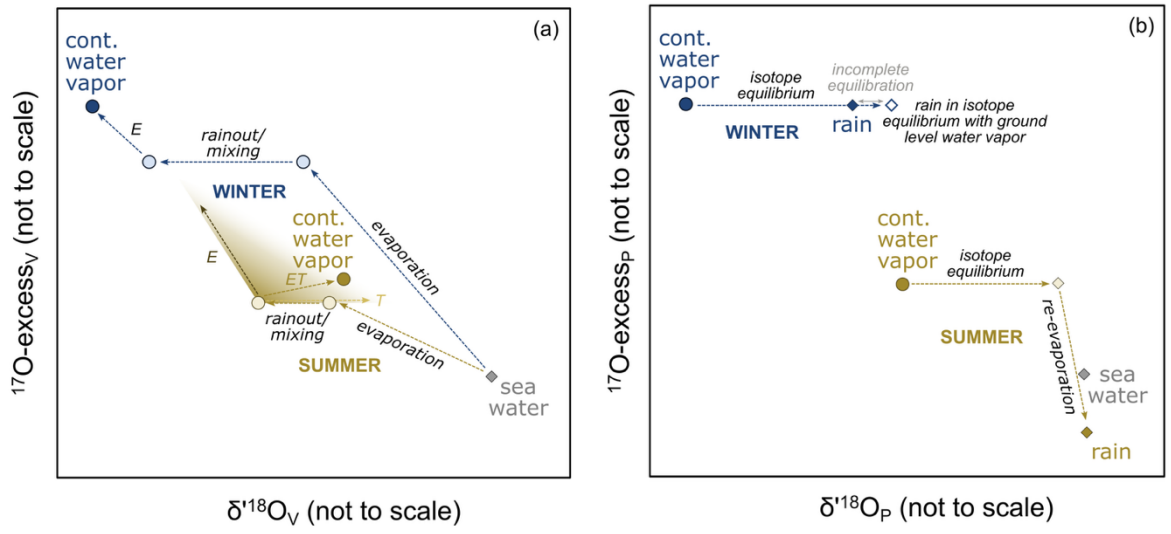

Figure 6: Synthesis of the effect of ocean evaporation, rainout, air mass mixing, continental moisture recycling (ET) and post formation precipitation processes in winter (blue) and summer (yellow) on the triple oxygen isotope composition of (a) atmospheric water vapor and (b) precipitation (see Sect. 4 for further details).

4.1 Evaporative conditions at the oceanic moisture sources

The four identified oceanic moisture sources have lower RH_{SST} in winter than in summer, resulting in stronger kinetic fractionation during evaporation from the ocean and higher d-excess$_V$ and ^{17}O-excess$_V$ in the evaporated water vapor in winter than in summer (Fig. 5). This seasonal change is clearly visible in the d-excess$_V$ measured at O_3HP and to a lesser extent in the ^{17}O-excess$_V$. This consistency suggests that seasonal changes in ocean evaporative conditions at the moisture sources drives seasonal changes in the isotopic composition of atmospheric water vapor at the study site.

The four oceanic moisture sources show similar seasonal pattern in RH_{SST} and thus the isotope compositions of water vapor evaporated from these sources are similar. Therefore, different oceanic moisture source regions cannot be distinguished based on the isotope composition of atmospheric water vapor observed at our study site.

Changes in the evaporative conditions at the oceanic moisture sources have little impact on $\delta^{18}O_V$ and cannot explain the large seasonal variations observed at our study site. This indicates that $\delta^{18}O$ is likely modified by additional processes during air mass transport.

4.2 Rayleigh distillation during air mass transport

Along the air mass trajectory, the water vapor undergoes Rayleigh distillation due to the progressive rainout. Rainout is forced by a decrease in temperature, accompanied by a decrease of the atmospheric water mixing ratio and leads to a decrease of $\delta^{17}O$, $\delta^{18}O$ and $\delta^{2}H$ in atmospheric water vapor and subsequent precipitation (Dansgaard, 1964; Galewsky et al., 2016). Rayleigh distillation explains why the monthly average $\delta^{18}O_v$ at O_3HP is systematically lower than at the oceanic moisture sources (Fig. 5). The 2 to 3 ‰ lower $\delta^{18}O_V$ from the North Atlantic compared to Mediterranean sources reflects the magnitude

https://doi.org/10.5194/egusphere-2025-5879
Preprint. Discussion started: 5 December 2025

of Rayleigh distillation. The shorter distance of the study site from the Mediterranean than from the North Atlantic and less rainout along transport pathways implies smaller depletion in heavy isotopes and higher $\delta^{18}O_v$ (Delattre et al., 2015; Natali et al., 2021).

In contrast, Rayleigh distillation has limited impact on d-excess$_v$ and ^{17}O-excess$_v$ as these parameters are weakly sensitive to equilibrium isotope fractionation by definition (Merlivat & Jouzel, 1979; Xia et al., 2023). In mid-latitudes Rayleigh distillation is expected to cause up to 3 ‰ changes in d-excess$_v$, with the direction of change depending on the season and the degree of distillation (Xia et al., 2022). The effect should not exceed a 5 per meg increase for ^{17}O-excess$_v$ (Xia et al., 2023).

Although d-excess$_v$ measured at the O_3HP is close to d-excess$_v$ estimates at the oceanic moisture sources, as expected for Rayleigh distillation,^{17}O-excess$_v$ is systematically higher by 15 per meg. This inconsistency may result from an inaccurate ^{17}O-excess average value used for sea water (-5 per meg) in the calculation of ^{17}O-excess$_v$ above the oceanic moisture sources. To date, the dataset of ^{17}O-excess in seawater is limited (Lin et al., 2021; Luz & Barkan, 2010), so that estimates of oceanic ^{17}O-excess$_v$ are not very accurate. Additionally, processes such as the aerodynamic condition over oceans and the incorporation of water vapor from other sources into the seawater boundary layer can affect the isotopic composition of seawater evaporation fluxes (Xia et al., 2023).

4.3 Terrestrial moisture recycling

The contribution of evaporation from continental surface waters (lakes, rivers, soils, etc.) and plant transpiration fluxes to the atmospheric water vapor can influence its isotope composition. Assuming the continental surface water has an isotopic composition close to that of precipitation, the contribution of continental evaporation to the atmosphere decreases $\delta^{18}O_v$ and increases d-excess$_v$ and ^{17}O-excess$_v$ (Craig & Gordon, 1965; Rothfuss et al., 2021). Plant transpiration is assumed to be non-fractionating relative to soil water (Galewsky et al., 2016 and references therein). Therefore, assuming soil water reflects the isotopic composition of precipitation, the contribution of plant transpiration fluxes to the atmosphere increases $\delta^{18}O_v$ but has only little impact on ^{17}O-excess$_v$ and d-excess$_v$. In total, net evapotranspiration affects $\delta^{18}O_v$, with the direction and magnitude depending on the relative contributions of evaporation and transpiration, whereas d-excess$_v$ and ^{17}O-excess$_v$ are elevated only when evaporation is substantial.

The low $\delta^{18}O$ and high monthly average ^{17}O-excess$_v$ measured at the study site relative to the oceanic vapor could result from a contribution of continental evaporation. However, the similarity between the d-excess$_v$ measured on site and estimated at oceanic moisture sources contradicts this possibility and instead argues for a poor estimate of ^{17}O-excess$_v$ above the ocean. Terrestrial moisture recycling is difficult to decipher on the regional scale as the isotope composition of atmospheric water vapor integrates several processes occurring along the air mass transport pathway. In contrast, the contribution of local evapotranspiration is resolved in diurnal variations in the isotope composition of atmospheric water vapor.

https://doi.org/10.5194/egusphere-2025-5879
Preprint. Discussion started: 5 December 2025

Higher q below the canopy, lower $\delta^{18}O_V$ and higher d-excess$_V$ and ^{17}O-excess$_V$ during the day (with a peak in the afternoon) than at night is consistent with a daytime contribution from local evapotranspiration. The fact that this day-night isotopic pattern is more pronounced during the forest growth period (Fig. 3) supports the impact of both soil evaporation and plant transpiration. Day-night variations in d-excess$_V$ have been reported across diverse environments, including forests, grasslands, wetlands, agricultural areas and urban regions (Berkelhammer et al., 2013; Delattre et al., 2015; Welp et al., 2012). In addition to local evapotranspiration fluxes that lead to high d-excess$_V$ during the day (Huang & Wen, 2014; Simonin et al., 2014; Welp et al., 2012; Zhao et al., 2014), low nocturnal d-excess$_V$ values have been linked to plant-atmosphere water exchange (Bastrikov et al., 2014; Lai & Ehleringer, 2011; Simonin et al., 2014), and dewfall (Bastrikov et al., 2014; Berkelhammer et al., 2013). Although plant transpiration decreases during night, incomplete stomata closure allows continued equilibrium isotope exchange between evaporated leaf water and the atmosphere under high relative humidity (Berkelhammer et al., 2013), leading to higher $\delta^{18}O_V$ and lower d-excess$_V$ and ^{17}O-excess$_V$. The entrainment of the residual layer or air from the lower free troposphere into the planetary boundary layer may contribute to high daytime d-excess$_V$ values (Lai & Ehleringer, 2011; Simonin et al., 2014). However, the low q of the lower free troposphere (< 4 kppmv) limits its influence on the isotope composition of atmospheric water vapor during downward mixing. In addition, Rayleigh distillation during adiabatic air ascent and air mass mixing, which drives the isotopic composition of the lower free troposphere (e.g., H. He & Smith, 1999; Salmon et al., 2019; Sodemann et al., 2017), is not expected to significantly influence ^{17}O-excess$_V$.

4.4 Mixing between air masses

The mixing of air masses from different origins frequently occurs during atmospheric transport. Its effect on ^{17}O-excess$_V$ differs from that on d-excess$_V$ due to its logarithmic (non-linear) δ' notation (Li et al., 2015; Aron et al., 2021; Leuenberger and Ranjan, 2021). The mixing of two air masses with different $\delta^{18}O_V$ but similar ^{17}O-excess$_V$ and d-excess$_V$ results in a decrease in ^{17}O-excess$_V$, while d-excess$_V$ remains largely unchanged. This decrease in ^{17}O-excess$_V$ is however small, representing only 3 per meg for a $\delta^{18}O_V$ difference of 10 ‰ between two air masses with the same water content (Xia et al., 2023). As isotopic differences in atmospheric water vapor between the four identified oceanic moisture sources are small, mixing during air mass transport is unlikely to significantly alter the isotopic composition of atmospheric water vapor observed at the O_3HP site.

4.5 Precipitation formation, raindrop re-evaporation, and isotopic (dis)equilibrium with atmospheric water vapor

Precipitation, either liquid or solid, forms in isotope equilibrium with atmospheric water vapor at cloud height, which is typically depleted in heavy isotopes compared to near-surface atmospheric water vapor due to Rayleigh distillation (Giménez et al., 2021 and references therein; Salmon et al., 2019; Sodemann et al., 2017). As raindrops fall through the air column, they continuously exchange water molecules with the surrounding vapour and equilibrate isotopically. This is the basis for the isotope equilibrium assumption between precipitation and near-surface atmospheric water vapor. At O_3HP during winter

https://doi.org/10.5194/egusphere-2025-5879
Preprint. Discussion started: 5 December 2025

months, $\delta^{18}O_V$ is slightly higher than $\delta^{18}O_{Veq}$ and the two snowfall events have the largest $\Delta^{18}O_{Veq\text{-}V}$ (-12.3‰) (Fig. 4). These differences suggest that atmospheric water vapor is more enriched at ground level than at the height of rain formation, and that equilibration during raindrop falling is incomplete. Indeed, equilibration rates are hampered under cold conditions, and no equilibration occurs between vapor and solid (Graf et al., 2019). Incomplete equilibration can also occur when low q in the atmosphere is associated with strong vertical isotope gradients in atmospheric water vapor, when drops are large or precipitation forms at high altitude (Graf et al., 2019; Penchenat et al., 2020). This incomplete equilibration has little effect on $d\text{-excess}_P$ (average deviation -0.8 ± 3.0 ‰) due to the generally small vertical gradients of $d\text{-excess}_V$ in the lowermost troposphere (Salmon et al., 2019; Sodemann et al., 2017). Notably, in winter, $^{17}O\text{-excess}_P$ is always close to $^{17}O\text{-excess}_V$ rather than 10–15 per meg lower as expected from isotope equilibrium (Fig. 4). The reason for this offset remains unclear so far.

During spring and summer months, the systematic correlation between $\Delta\delta^{18}O_{Veq\text{-}V}$, $\Delta d\text{-excess}_{Veq\text{-}V}$ and $\Delta^{17}O\text{-excess}_{Veq\text{-}V}$ (Fig. 4) suggests the impact of re-evaporation on precipitation. Rain re-evaporation has been found to occur under unsaturated conditions in mid-latitude to tropical regions (Aemisegger et al., 2015; Aemisegger & Sjolte, 2018; Graf et al., 2019; Landais et al., 2010; Mercer et al., 2020). Indeed, positive $\Delta\delta^{18}O_{Veq\text{-}V}$ values at O_3HP occur when RH is lower than 90 %. The fact that there are no isotopic differences in atmospheric water vapor between rainy and non-rainy days (data not shown) implies that rain re-evaporation does not significantly affect atmospheric water vapor. The contribution of plant transpiration and soil evaporation to the near-surface atmospheric water vapor may emphasize the isotope disequilibrium between precipitation and atmospheric water vapor in summer. At annual scale, the opposing winter and summer monthly $\Delta^{18}O_{Veq\text{-}V}$ values effectively cancel each other, so that $\delta^{18}O_{Veq}$ closely approximates $\delta^{18}O_V$ (cf., Voigt et al., 2023).

5 Conclusion

This study provides a unique dataset of the triple oxygen and hydrogen isotope composition of atmospheric water vapor and precipitation in a Mediterranean forest ecosystem, highlighting seasonal and diurnal changes and the processes driving it. Our results demonstrate that ^{17}O-excess and d-excess are principally driven by evaporation processes, while primary isotope values (δ^2H_V, $\delta^{17}O_V$, $\delta^{18}O_V$) mainly reflect rainout along the atmospheric transport pathway.

On a seasonal scale, $^{17}O\text{-excess}_V$ and $d\text{-excess}_V$ reflect evaporative conditions in the oceanic moisture sources. Lower winter RH_{SST} enhances kinetic fractionation during ocean evaporation, producing water vapor with ~2 ‰ higher $d\text{-excess}_V$ and ~7 per meg higher $^{17}O\text{-excess}_V$ than in summer. Different oceanic moisture sources and weather regimes could, however, not be resolved likely due to the frequent mixing of sources with only weak isotopic differences resulting from similar RH_{SST}. This contrasts with previous findings that linked higher $d\text{-excess}_P$ observed in Mediterranean compared to North Atlantic sources to differences in RH_{SST} (Casellas et al., 2019; Celle-Jeanton et al., 2001; Cruz-San Julian et al., 1992; Delattre et al., 2015; Natali et al., 2021). Lagrangian moisture source diagnostic can help to quantify and better disentangle moisture source contributions (Sodemann et al., 2008). Simultaneous measurements of ^{17}O-excess and d-excess in seawater and atmospheric

https://doi.org/10.5194/egusphere-2025-5879
Preprint. Discussion started: 5 December 2025

water vapor over the Atlantic Ocean and the Mediterranean Sea are needed to clarify isotopic source contrasts and refine paleoclimate interpretations.

On diurnal scale, increases in $^{17}O\text{-excess}_V$ and $d\text{-excess}_V$ during daytime reflect the impact of local evapotranspiration, while nighttime decreases result from continued isotopic exchange between leaf water and ambient vapor likely due to incomplete stomata closure. Because these opposing signals largely offset on daily scale, local and regional evapotranspiration effects are not evident in monthly averages. Triple oxygen isotope measurements of atmospheric water vapor thus provide a valuable tool to disentangle transpiration and evaporation signals, ultimately improving the understanding of land-atmosphere water exchange across diverse climate and vegetation contexts.

Summer precipitation shows strong coupling between $\delta^{18}O_P$, $^{17}O\text{-excess}_P$ and $d\text{-excess}_P$ indicating rain re-evaporation, while negative $\Delta\delta^{18}O_{Veq\text{-}V}$ values in winter suggest incomplete isotope equilibration with ambient vapor. Although precipitation frequently deviates from isotopic equilibrium with near-surface atmospheric water vapor at the event scale, equilibrium water vapor reliably approximates near-surface isotope composition at monthly or annual scale. Thus, isotope-based reconstructions for model validation are robust for the studied climate context, but mechanistic models assuming short-term isotope equilibrium between water vapor and precipitation should incorporate associated uncertainties.

Our findings have also direct implications for interpreting long-term isotopic records of rain preserved in paleoclimate archives. The triple oxygen and hydrogen isotope composition of such record can help to (i) reconstruct past changes in ocean evaporative conditions, (ii) infer variations in atmospheric circulation and air mass mixing, provided that the different sources have distinct RH_{SST} values, and (iii) identify dry periods through evidence of rain re-evaporation. Overall, triple oxygen isotope measurements of precipitation provide a means to quantify the relative influence of these processes, helping to better understand the impact of climate change at regional and local levels.

Appendices

Appendix A

https://doi.org/10.5194/egusphere-2025-5879
Preprint. Discussion started: 5 December 2025

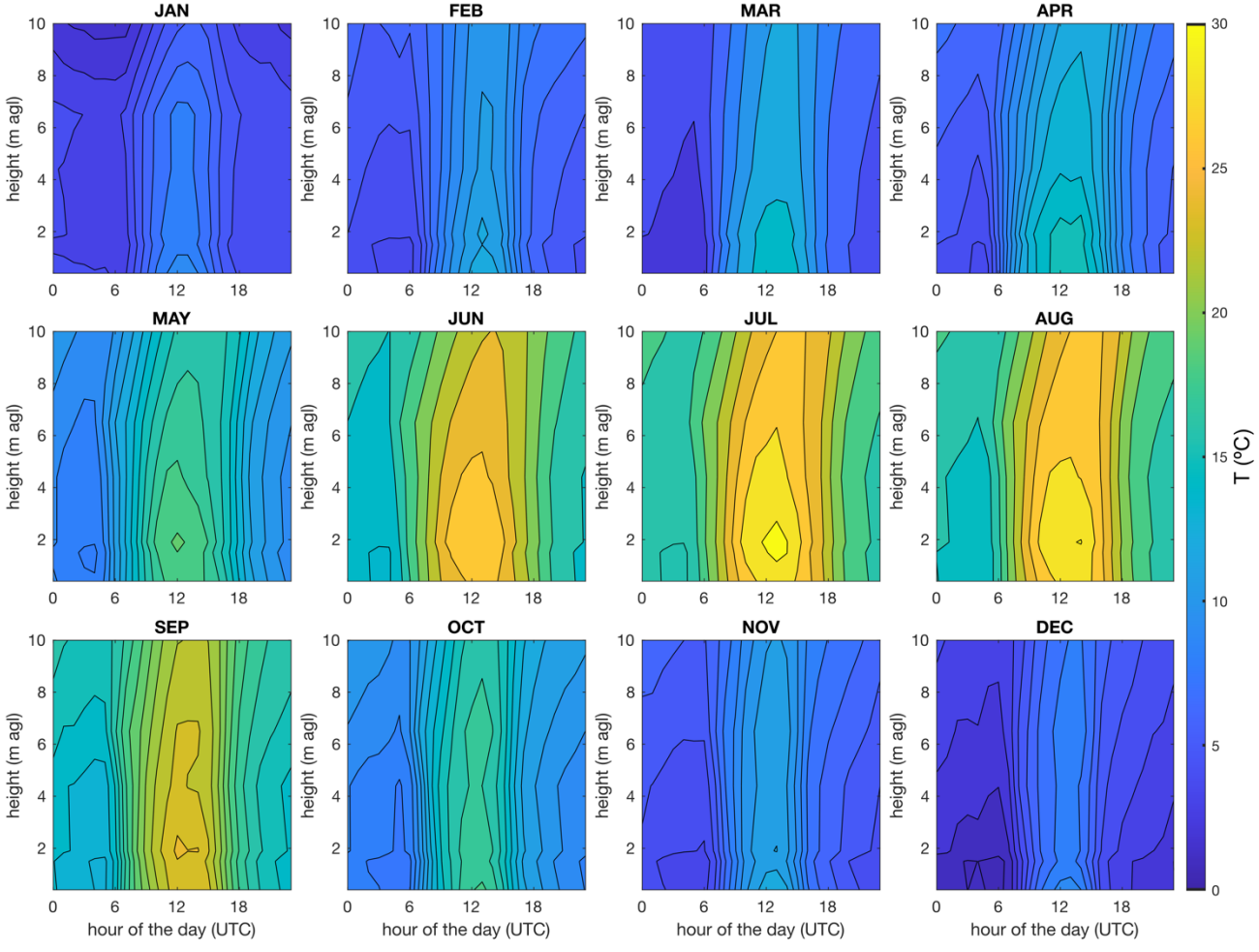

500

Figure A1: Monthly average variability of atmospheric temperature in the near-surface atmosphere over the day. Temperature measurements at 0.4 m, 1.5 m, 1.9 m, 4.4 m 6.15 m and 10 m agl were obtained from the O_3HP database (Reiter et al., 2015). Data were linearly interpolated between measurement heights, and the hourly means were computed for each month.

https://doi.org/10.5194/egusphere-2025-5879
Preprint. Discussion started: 5 December 2025

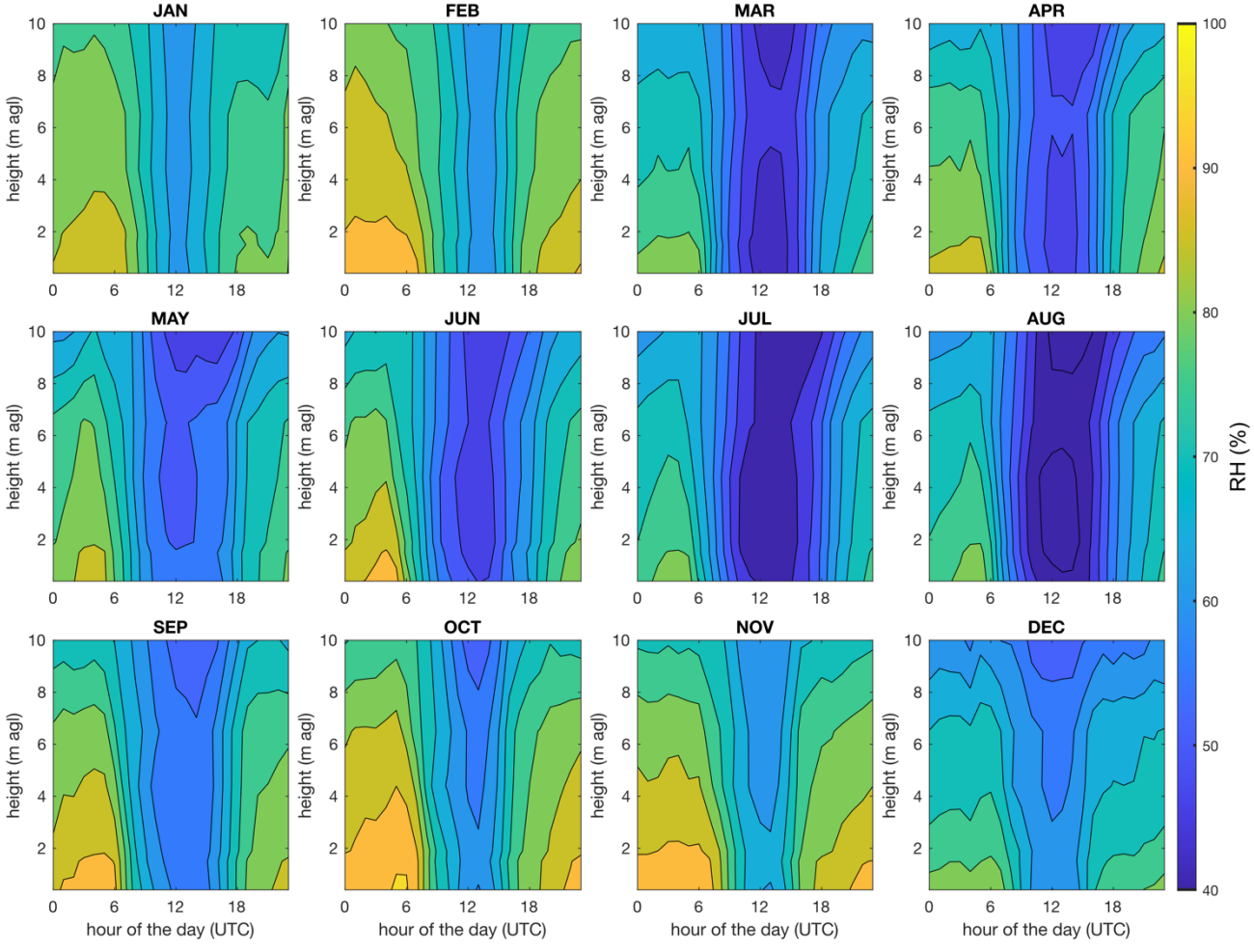

Figure A2: Monthly average variability of atmospheric relative humidity in the near-surface atmosphere over the day. Relative humidity measurements at 0.4 m, 1.5 m, 1.9 m, 4.4 m 6.15 m and 10 m agl were obtained from the O_3HP database (Reiter et al., 2015). Data were linearly interpolated between measurement heights, and the hourly means were computed for each month.

https://doi.org/10.5194/egusphere-2025-5879
Preprint. Discussion started: 5 December 2025

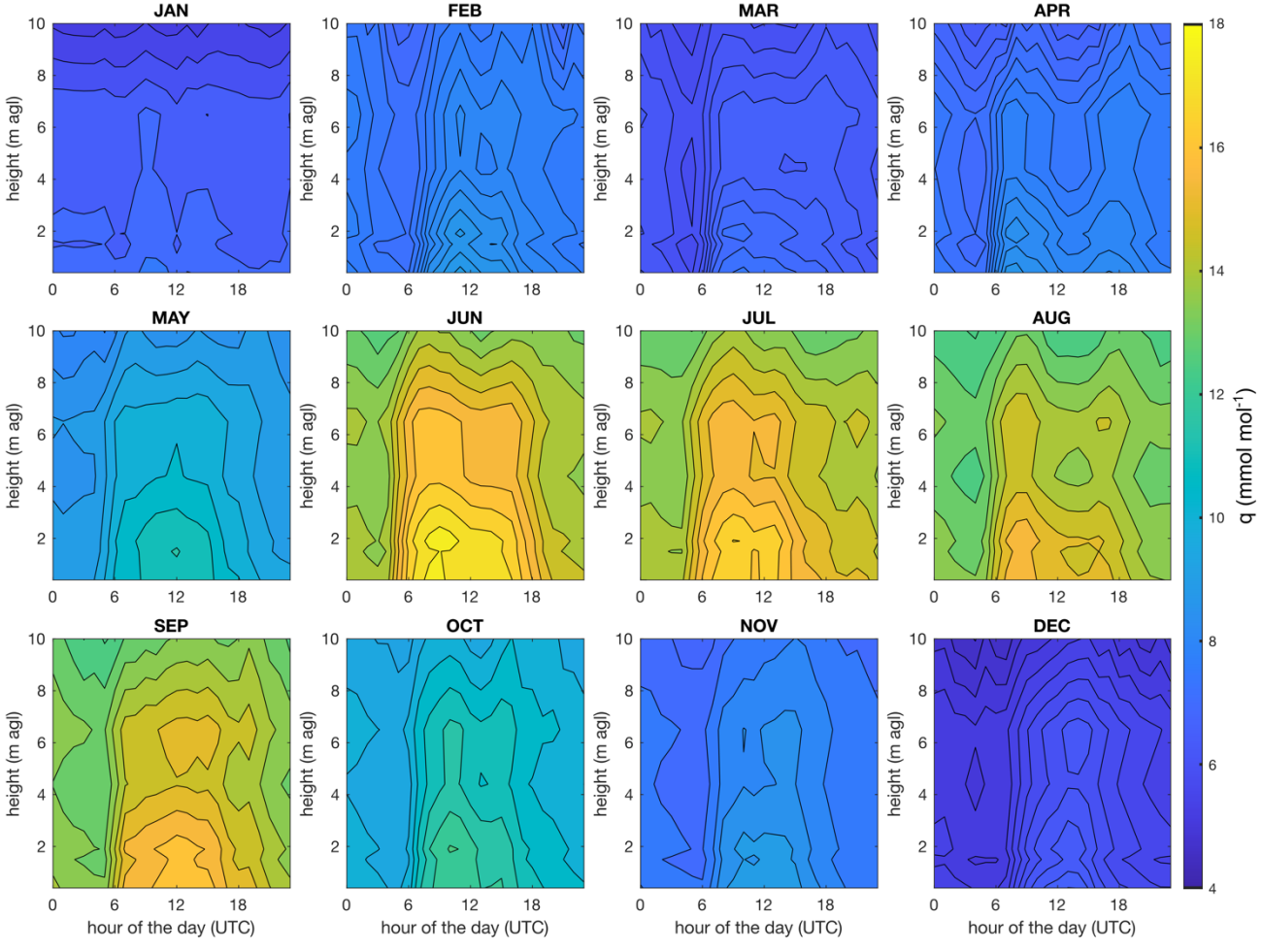

Figure A3: Monthly average variability of the atmospheric water mixing ratio in the near-surface atmosphere over the day. Measurements of atmospheric temperature and relative humidity at 0.4 m, 1.5 m, 1.9 m, 4.4 m 6.15 m and 10 m agl were obtained from the O_3HP database (Reiter et al., 2015). The atmospheric water mixing ratio was calculated from these data, linearly interpolated between heights, and averaged hourly for each month.

https://doi.org/10.5194/egusphere-2025-5879
Preprint. Discussion started: 5 December 2025

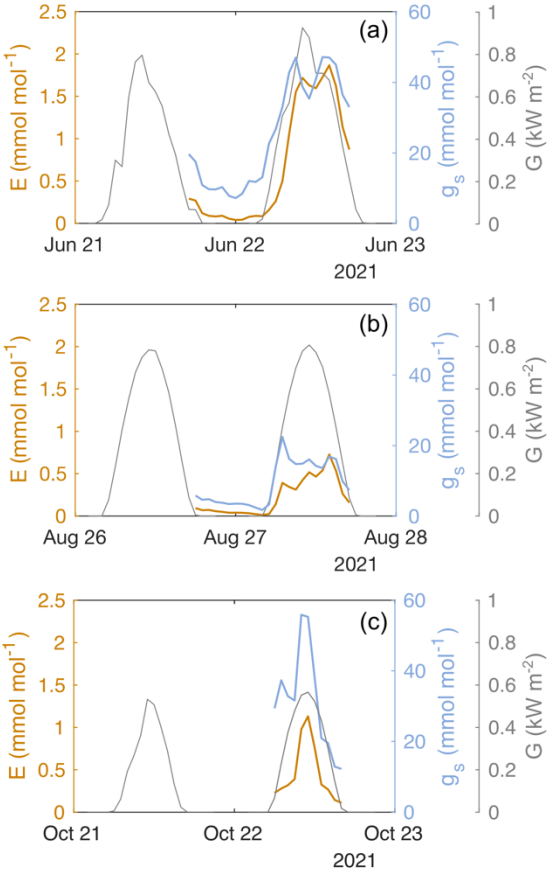

520 **Figure A4:** Diurnal evolution of transpiration (E) and stomatal conductance (g_s) of individual oak leaves in the sun-crown of the forest canopy in different stages of the oak forest growing season: (a) early stage, (b) dry stage, (c) last stage. The diurnal cycle of global solar radiation (G, grey curve) is shown for comparison.

https://doi.org/10.5194/egusphere-2025-5879
Preprint. Discussion started: 5 December 2025

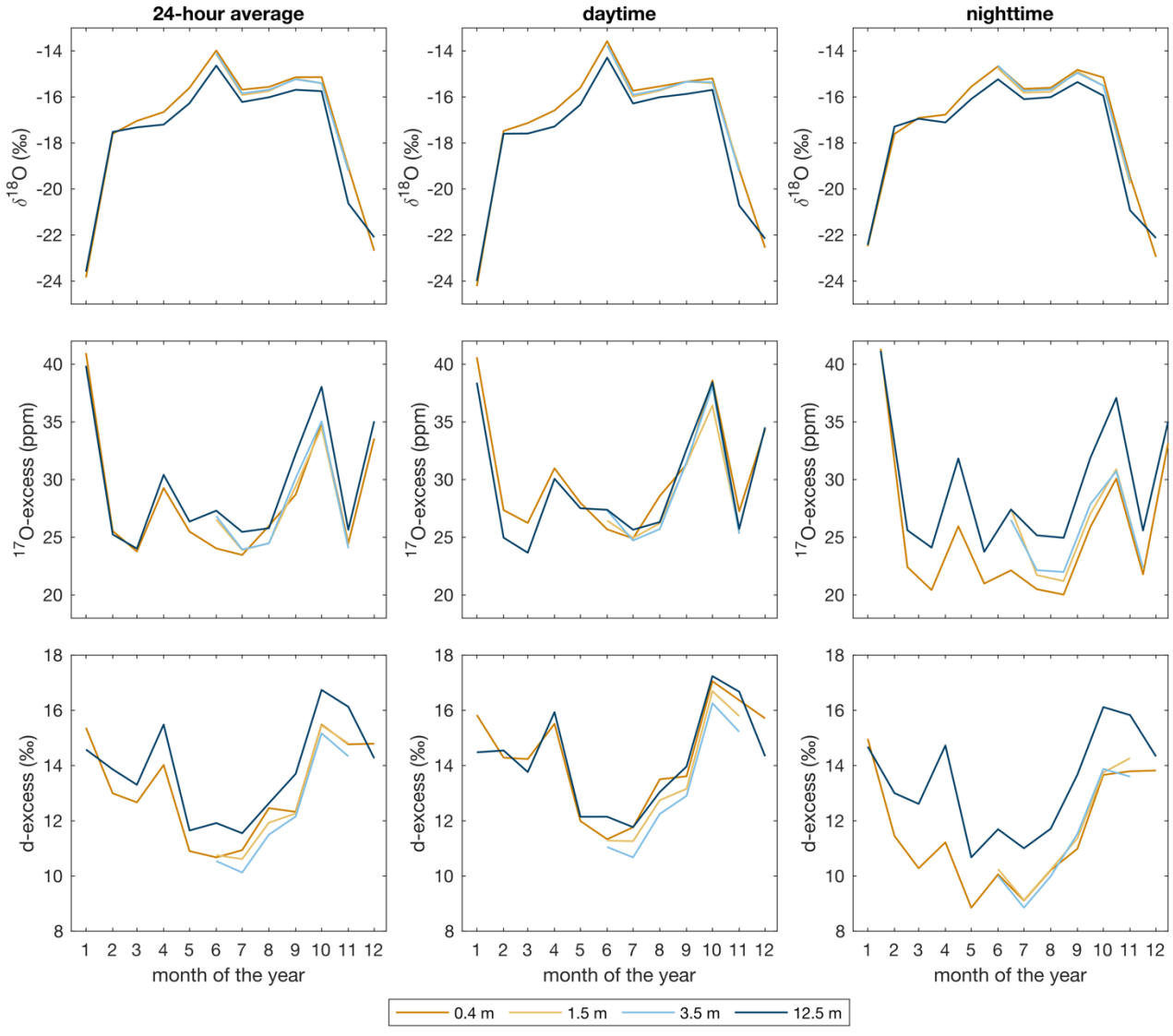

525

Figure A5: Monthly average of $\delta^{18}O$, ^{17}O-excess and d-excess of atmospheric water vapor at different heights above ground level (agl) in 2021 for daily, daytime and night-time conditions. Atmospheric water vapor at 1.5 and 3.5 m agl was monitored continuously only from June to November 2021, in relation to the oak forest growing season. Therefore, for these heights no isotope data is available from January to May and December 2021.

https://doi.org/10.5194/egusphere-2025-5879
Preprint. Discussion started: 5 December 2025

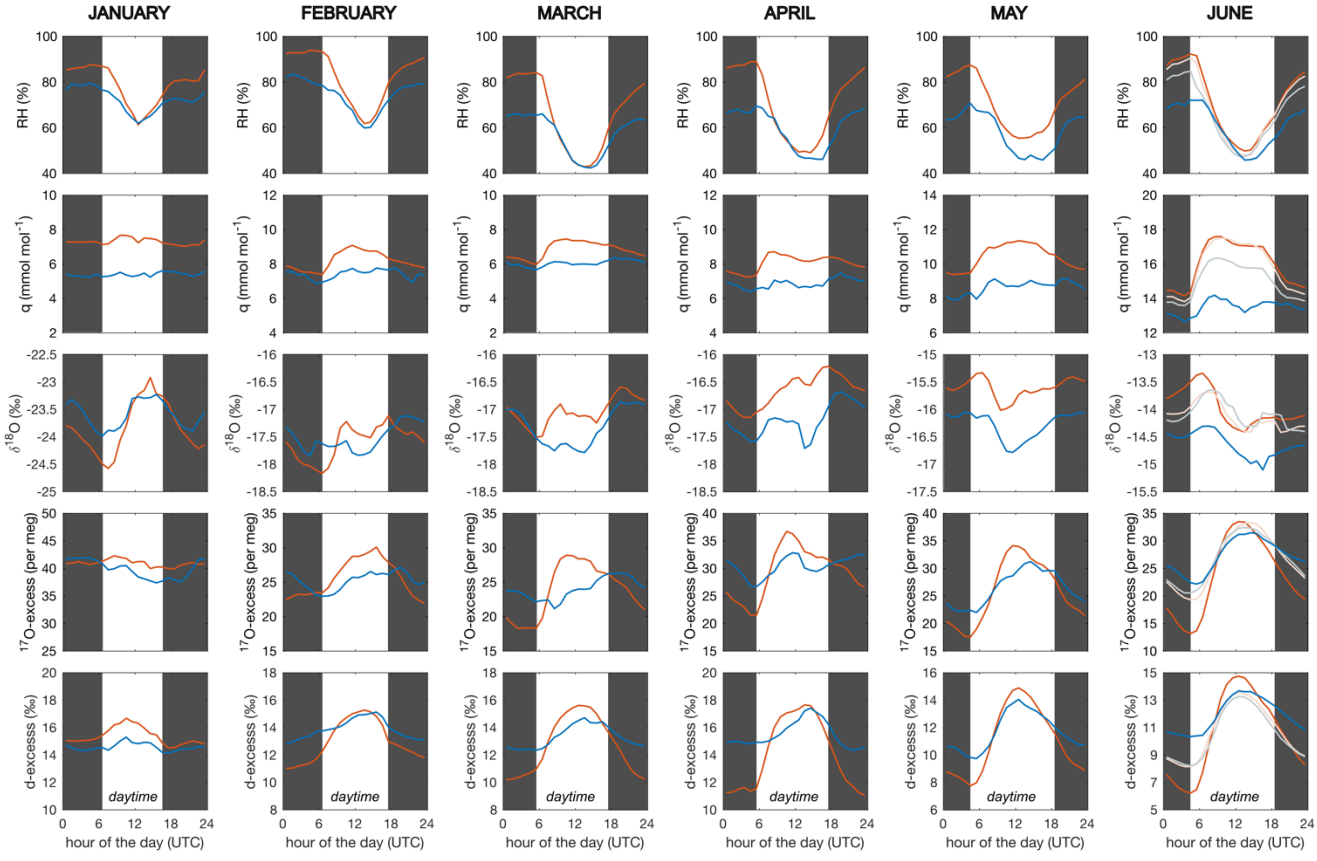

Figure A6: Monthly average diurnal cycle of relative humidity (RH), atmospheric water mixing ratio (q) and $\delta^{18}O$, d-excess and ^{17}O-excess of atmospheric water vapor at different measurements heights above the grass plot (red) and below (pale), within (grey) and above (blue) the oak forest canopy for January to June 2021. The grey shaded areas indicate the night-time periods.

https://doi.org/10.5194/egusphere-2025-5879
Preprint. Discussion started: 5 December 2025

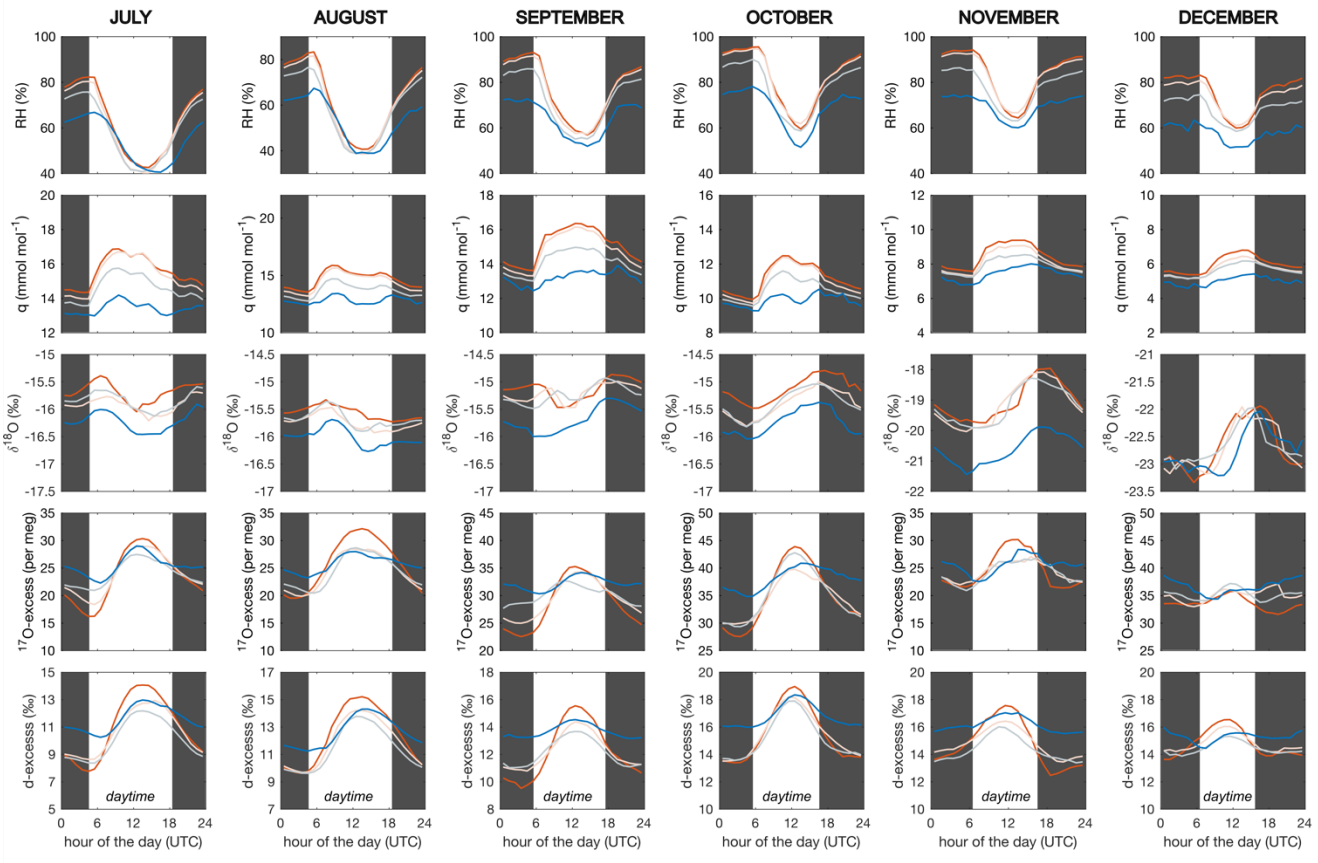

535 **Figure A7:** Same as figure A7, but for July to December 2021.

https://doi.org/10.5194/egusphere-2025-5879
Preprint. Discussion started: 5 December 2025

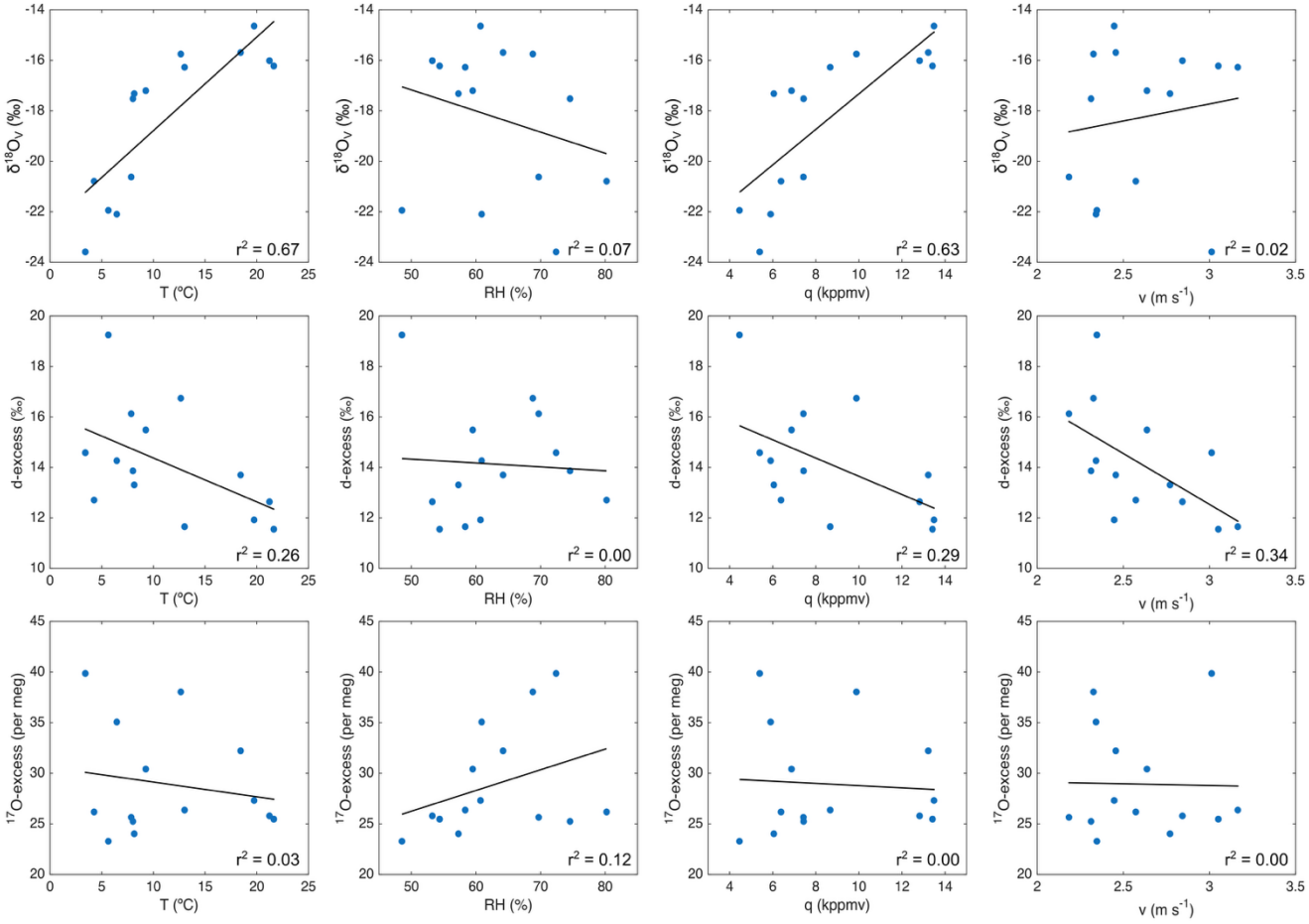

Figure A8: Correlations observed between monthly average $\delta^{18}O$, d-excess and ^{17}O-excess of atmospheric water vapor measured at 12.5 m agl and relative humidity (RH), atmospheric temperature (T_{air}), the atmospheric water mixing ratio (q) and wind speed (v) at 10 m agl.

https://doi.org/10.5194/egusphere-2025-5879
Preprint. Discussion started: 5 December 2025

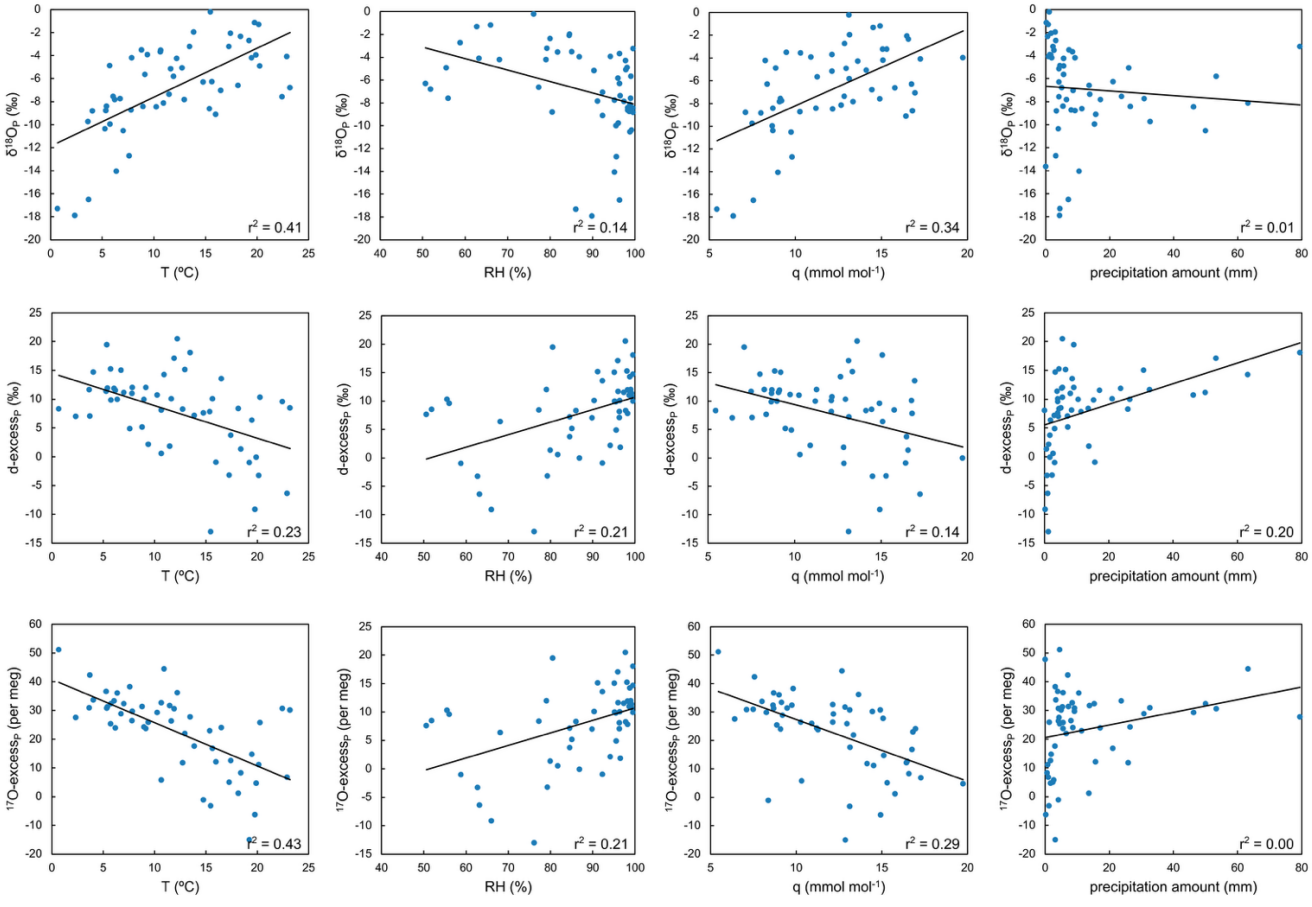

Figure A9: Correlations observed between event-based $\delta^{18}O$, d-excess and ^{17}O-excess of precipitation and relative humidity (RH), atmospheric temperature (T_{air}), the atmospheric water mixing ratio (q) and precipitation amount.

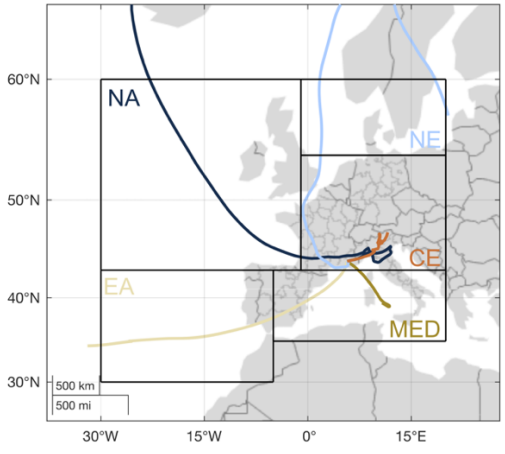

Figure A10: Mean 168-hour air mass back trajectories calculated for every hour of each day in 2021, clustered by air mass origin. NA = North Atlantic, EA = East Atlantic, MED = Mediterranean Sea, CE = Continental Europe, and NE = Northern Europe.

https://doi.org/10.5194/egusphere-2025-5879
Preprint. Discussion started: 5 December 2025

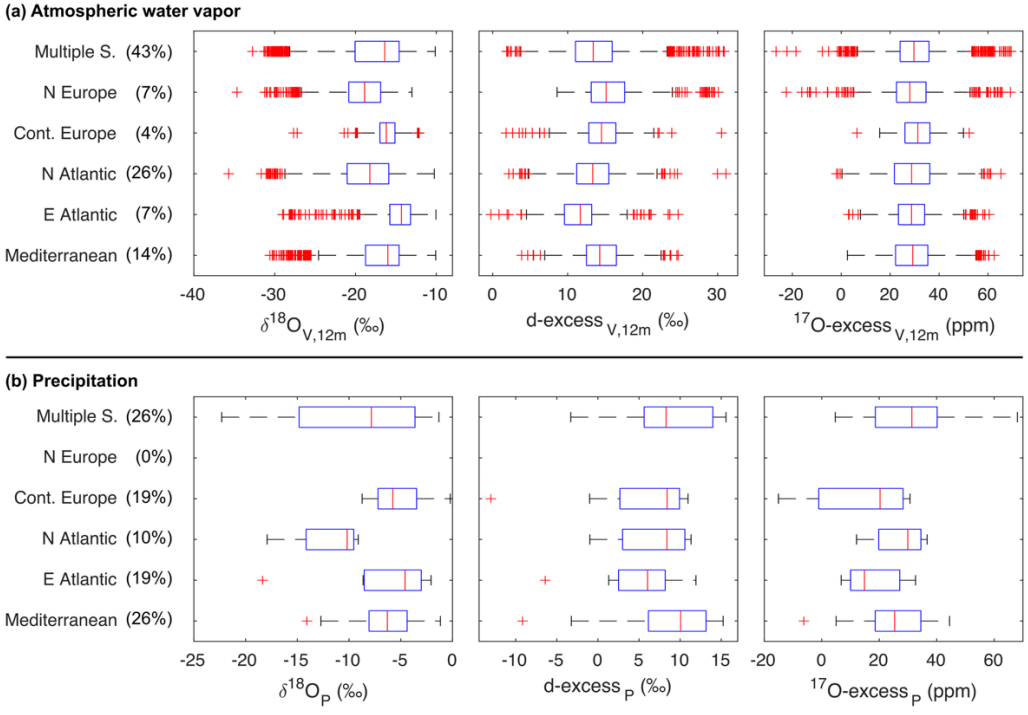

Figure A11: Box plots of isotope compositions of (a) atmospheric water vapor at 12.5 m agl and (b) precipitation for identified oceanic moisture sources. The red center mark indicates the median, and the lower and upper ends of the box indicate the 25th and 75th percentiles, respectively. The whiskers extend to the most extreme data points that are not considered outliers, and outliers are represented individually by the '+' marker symbol. The numbers in brackets following the moisture source names indicate (a) the percentage of occurrence and (b) total precipitation amount of each moisture source.

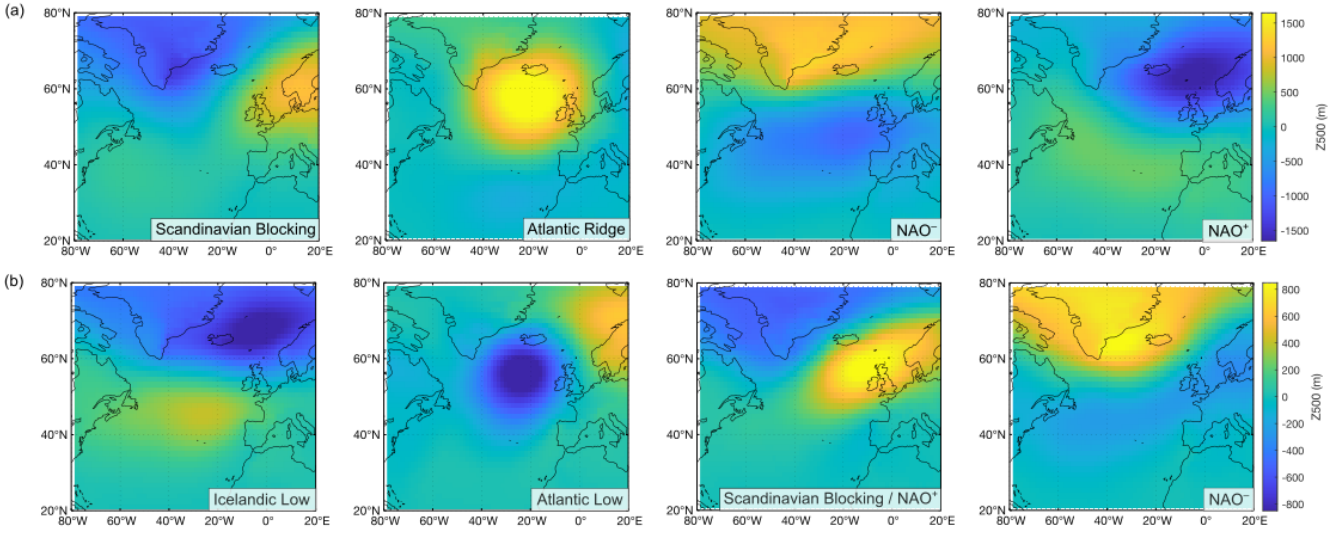

https://doi.org/10.5194/egusphere-2025-5879
Preprint. Discussion started: 5 December 2025

Figure A12: Centroids of (a) the four wintertime and (b) the four summertime weather regimes obtained from daily anomalous geopotential height at the 500-hPa altitude (Z500, colour) from the European Centre for the Medium-Range Weather Forecasts (ECMWF) ERA5 reanalysis over 1989–2022. In winter, the Atlantic Ridge regime is associated with a high-pressure system over the Atlantic Ocean, driving strong northwesterly winds (Mistral) and resulting in cool, dry conditions in the Mediterranean region (Vautard, 1990). The NAO– regime emerges when the Icelandic low shifts southward, displacing the Atlantic jet stream to lower latitudes and inducing southerly winds that bring warmer, wetter conditions to the Mediterranean (Cassou et al., 2004). In contrast, the NAO+ regime is characterized by a strong pressure gradient between the Icelandic Low and the Azores High, promoting westerly to northwesterly winds and generally dry conditions in the Mediterranean (Cassou et al., 2004). The Scandinavian Blocking regime involves a persistent anticyclone over the Scandinavian Peninsula, preventing low pressure systems reaching Europe and leads to north-easterly winds across the western Mediterranean. In summer, the Blocking/NAO+ regime resembles a blocking-like pattern, with a high-pressure anomaly over Scandinavia and the North Sea. The Atlantic Low is dominated by a low-pressure system over the North Atlantic, accompanied by weaker positive anomalies extending toward Scandinavia, facilitating the advection of warm air masses from northern Africa and the Mediterranean basin (Cassou et al., 2005). The summer NAO– regime is characterized by a low-pressure anomaly over the British Isles and a strong high-pressure anomaly over Greenland, while the Icelandic Low regime displays a dipole pattern with a low-pressure anomaly between Iceland and Scandinavia and a weak high-pressure anomaly over the North Atlantic.

https://doi.org/10.5194/egusphere-2025-5879
Preprint. Discussion started: 5 December 2025

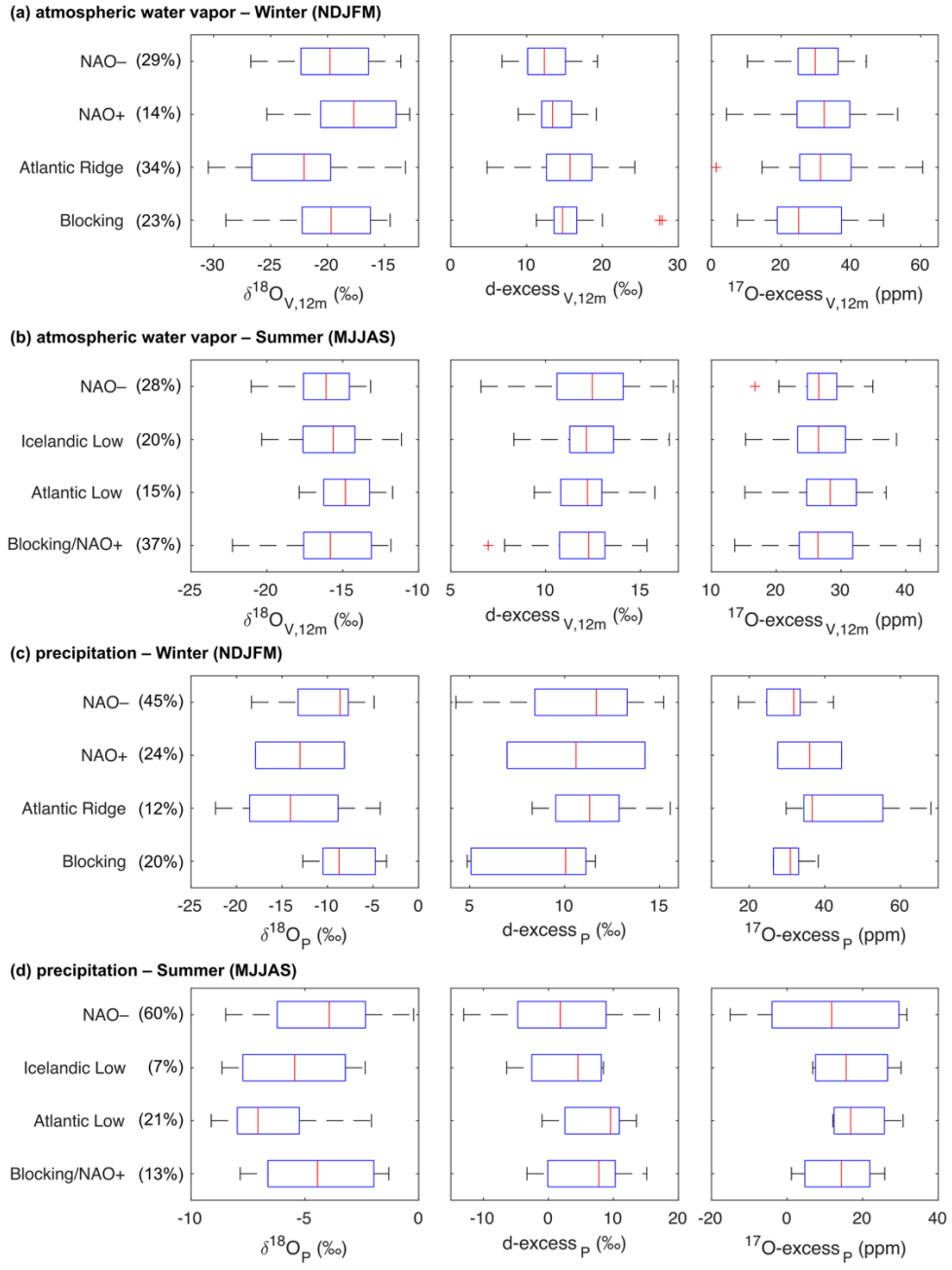

Figure A13: Box plots of isotope compositions of (a)-(b) atmospheric water vapor and (c)-(d) precipitation for the four wintertime and the four summertime weather regimes. The red center mark indicates the median, and the lower and upper ends of the box indicate the 25th and 75th percentiles, respectively. The whiskers extend to the most extreme data points that are not considered outliers, and outliers are represented individually by the '+' marker symbol. The numbers in brackets behind the weather regime names indicate (a)-(b) the percentage of occurrence and (c)-(d) the total precipitation amount of each weather regime.

https://doi.org/10.5194/egusphere-2025-5879
Preprint. Discussion started: 5 December 2025

Appendix B

Table B1: Sample name, sample type, sampling date and isotope composition of meteoric waters collected in this study. Samples from springs, wells and rivers in the surroundings of the study site were collected seasonally. Precipitation was collected monthly from June 2019 to December 2020, but on quasi-event scale in 2021. Given isotope values for precipitation in 2021 represent amount-weighted monthly averages. In addition, the amount-weighted average isotope values and standard deviations for precipitation in 2020, 2021 and over the whole dataset are given.

Sample name	Sample type	Sampling date	$\delta^{18}O$ (‰)	$\delta'^{18}O$ (‰)	$\delta^{2}H$ (‰)	^{17}O-excess (per meg)	d-excess (‰)	Precipitation amount (mm)
Lavoir Barri	spring	Dec-20	-7.8	-7.8	-50.3	33	11.7	–
Lavoir Barri	spring	Apr-21	-7.7	-7.7	-49.8	37	11.9	–
Lavoir Barri	spring	Jun-21	-7.7	-7.7	-49.8	28	11.9	–
Lavoir Barri	spring	Aug-21	-7.7	-7.8	-50.2	28	11.8	–
Lavoir Barri	spring	Oct-21	-7.7	-7.8	-50.1	26	11.9	–
Lavoir Marceline	spring	May-20	-7.2	-7.2	-47.3	27	10.4	–
Lavoir Marceline	spring	Dec-20	-7.4	-7.4	-48.1	33	11.1	–
Lavoir Marceline	spring	Apr-21	-7.4	-7.5	-48.3	32	11.1	–
Lavoir Marceline	spring	Jun-21	-7.4	-7.4	-47.8	37	11.2	–
Lavoir Marceline	spring	Aug-21	-7.4	-7.4	-48.0	20	11.1	–
Lavoir Marceline	spring	Oct-21	-7.0	-7.0	-45.1	26	10.9	–
Puits jardin	well	Dec-20	-7.2	-7.2	-46.4	27	11.1	–
Puits jardin	well	Apr-21	-7.2	-7.2	-46.8	28	10.7	–
Puits jardin	well	Jun-21	-7.0	-7.1	-45.8	30	10.6	–
Puits jardin	well	Aug-21	-7.0	-7.1	-45.8	26	10.5	–
Puits jardin	well	Oct-21	-6.9	-6.9	-45.1	27	10.3	–
Source enterrée	spring	Dec-20	-6.1	-6.1	-38.4	33	10.2	–
Source enterrée	spring	Jun-21	-7.4	-7.4	-46.9	33	12.5	–
Source enterrée	spring	Aug-21	-7.3	-7.3	-45.9	20	12.2	–
Source enterrée	spring	Oct-21	-5.8	-5.9	-35.8	23	11.0	–
Riviere Largue	river	May-20	-7.3	-7.4	-47.1	34	11.6	–
Riviere Largue	river	Dec-20	-7.5	-7.5	-48.7	28	11.1	–
Riviere Largue	river	Apr-21	-7.5	-7.6	-49.0	26	11.2	–
Riviere Largue	river	Jun-21	-7.5	-7.6	-48.7	27	11.5	–
Riviere Largue	river	Aug-21	-7.4	-7.4	-48.3	22	11.1	–
Riviere Largue	river	Oct-21	-7.3	-7.3	-47.4	30	11.1	–
AV			**-7.3**		**-47.0**	**29**	**11.2**	–
SD			0.5		3.3	5	0.6	–
O_3HP	precipitation	Jun-19	-3.6	-3.6	-26.2	14	2.3	15
O_3HP	precipitation	Jul-19	-1.1	-1.1	-6.5	-1	2.3	64
O_3HP	precipitation	Aug-19	–	–	–	–	–	0
O_3HP	precipitation	Sep-19	-6.6	-6.6	-45.6	20	6.9	87
O_3HP	precipitation	Oct-19	-6.1	-6.1	-35.6	22	12.9	200
O_3HP	precipitation	Nov-19	-9.0	-9.0	-60.8	25	11.0	392
O_3HP	precipitation	Dec-19	-9.2	-9.2	-63.8	34	9.8	124
O_3HP	precipitation	Jan-20	-6.7	-6.7	-42.5	34	10.8	24
O_3HP	precipitation	Feb-20	–	–	–	–	–	0
O_3HP	precipitation	Mar-20	-7.0	-7.0	-49.3	29	6.8	39
O_3HP	precipitation	Apr-20	-5.5	-5.5	-32.2	29	12.0	40
O_3HP	precipitation	May-20	-6.4	-6.4	-41.3	20	9.9	150
O_3HP	precipitation	Jun-20	-5.1	-5.1	-35.4	14	5.2	65
O_3HP	precipitation	Jul-20	–	–	–	–	–	0
O_3HP	precipitation	Aug-20	-2.9	-2.9	-15.9	2	7.5	8
O_3HP	precipitation	Sep-20	-7.1	-7.1	-47.8	19	9.1	37
O_3HP	precipitation	Oct-20	-4.6	-4.6	-23.4	26	13.1	25
O_3HP	precipitation	Nov-20	-7.6	-7.7	-49.8	25	11.2	33
O_3HP	precipitation	Dec-20	-11.8	-11.9	-78.8	32	15.6	71
O_3HP	precipitation	Jan-21	-10.4	-10.4	-71.2	34	11.6	53
O_3HP	precipitation	Feb-21	-8.8	-8.8	-60.1	28	9.9	40
O_3HP	precipitation	Mar-21	-4.2	-4.2	-21.8	30	12.0	9
O_3HP	precipitation	Apr-21	-8.0	-8.0	-52.1	26	12.0	125
O_3HP	precipitation	May-21	-5.8	-5.8	-33.3	30	12.9	82

https://doi.org/10.5194/egusphere-2025-5879
Preprint. Discussion started: 5 December 2025

O_3HP	precipitation	Jun-21	-5.6	-5.6	-37.1	26	7.8	13
O_3HP	precipitation	Jul-21	-7.6	-7.6	-62.3	9	-1.4	21
O_3HP	precipitation	Aug-21	-7.0	-7.0	-47.9	5	8.2	58
O_3HP	precipitation	Sep-21	-5.7	-5.7	-36.2	14	9.2	70
O_3HP	precipitation	Oct-21	-3.3	-3.3	-8.2	28	18.2	85
O_3HP	precipitation	Nov-21	-8.6	-8.6	-55.8	41	12.8	85
O_3HP	precipitation	Dec-21	-11.1	-11.2	-78.5	30	10.6	88
amount-weighted AV		**2020**	**-7.0**		**-45.6**	**23**	**10.2**	**492**
amount-weighted SD			2.2		15.4	7	3.1	
amount-weighted AV		**2021**	**-7.5**		**-48.1**	**27**	**11.6**	**730**
amount-weighted SD			2.3		20.2	9	3.5	
amount-weighted AV		**ALL**	**-7.3**		**-48.1**	**24**	**10.6**	**2104**
amount-weighted SD			2.3		17.7	8	3.3	

Table B2: Monthly and annual average isotope composition of atmospheric water vapor at 12.5 m agl (V) and water vapor estimated from isotope equilibrium with monthly amount-weighted precipitation data (V_{eq}) for the period from January to December 2021.

Month	**$\delta^{18}O_V$ (‰)**		**$\delta^{2}H_V$ (‰)**		**d-excess$_V$ (‰)**		**^{17}O-excess$_V$ (per meg)**		**$\delta^{18}O_{Veq}$ (‰)**		**$\delta^{2}H_{Veq}$ (‰)**		**d-excess$_{Veq}$ (‰)**		**^{17}O-excess$_{Veq}$ (per meg)**	
	AV	**SD**	**AV**	**SD**	**AV**	**SD**	**AV**	**SD**	**AV**	**SD**	**AV**	**SD**	**AV**	**SD**	**AV**	**SD**
Jan	-23.6	4.4	-174	32	14.6	4.7	40	10	-21.5	4.9	-161	39	11.7	2.1	23	12
Feb	-17.5	3.7	-126	30	13.9	5.2	25	7	-19.5	4.0	-145	32	10.4	3.0	17	7
Mar	-17.3	3.2	-125	24	13.3	3.0	24	10	-15.0	–	-110	–	9.5	–	19	–
Apr	-17.2	2.5	-122	19	15.5	3.8	30	10	-18.6	1.0	-137	7	12.2	3.4	16	6
May	-16.3	2.1	-119	17	11.7	2.5	26	4	-16.0	1.0	-116	11	12.8	6.0	20	2
Jun	-14.6	2.3	-105	18	11.9	1.9	27	6	-15.3	2.4	-112	18	9.9	2.9	16	7
Jul	-16.2	2.3	-118	17	11.6	1.3	25	4	-17.1	2.5	-134	20	2.9	1.6	0	3
Aug	-16.0	2.3	-116	17	12.6	1.6	26	6	-16.5	0.8	-121	7	11.4	0.2	-4	9
Sep	-15.7	1.9	-112	15	13.7	1.7	32	4	-15.4	1.5	-113	8	10.8	4.4	4	8
Oct	-15.7	1.5	-109	12	16.7	1.9	38	9	-13.6	0.3	-93	2	16.0	0.6	18	2
Nov	-20.6	3.2	-149	24	16.1	2.5	26	12	-19.3	1.7	-142	15	12.9	2.9	30	6
Dec	-22.1	3.4	-163	26	14.3	2.8	35	8	-22.0	2.5	-164	22	12.1	2.1	19	6
Annual AV	**-17.7**	**2.8**	**-128**	**22**	**13.8**	**1.7**	**30**	**5**	**-17.8**	**2.7**	**-130**	**22**	**12.3**	**3.1**	**16**	**10**

Data availability

The dataset will be uploaded in an online data repository (PANGEAE).

Author contribution

CV, CVC, AA and CP designed the experiments and CV, IR, JPO and AA carried them out. CV developed the model code and performed the data analysis. FC did the statistical analysis. CC performed the classification of weather regimes. IXR provided meteorological data from the ICOS tower. CV prepared the manuscript with contributions from all co-authors.

https://doi.org/10.5194/egusphere-2025-5879
Preprint. Discussion started: 5 December 2025

Competing interests

The authors declare that they have no conflict of interest.

Acknowledgements

This study was conducted in the framework of the HUMI-17 project led by A.A. and supported by the ANR (ANR-17-CE01-0002-01), CNRS FR3098 ECCOREV, LABEX OT-Med, and OSU-Pytheas. It benefited from the CNRS resources allocated to the French ECOTRONS Research Infrastructure, from the Occitanie Region and FEDER investments as well as from the state allocation "Investissement d'Avenir" AnaEE-France ANR-11-INBS-0001. C.V. was supported by the Marie Curie-Sklodowska post-doctoral fellowship (#101063961).

References

Aemisegger, F., and Sjolte, J.: A climatology of strong large-scale ocean evaporation events. Part II: Relevance for the deuterium excess signature of the evaporation flux, J. Clim., 31, 7313–7336, https://doi.org/10.1175/JCLI-D-17-0592.1, 2018.

Aemisegger, F., Spiegel, J. K., Pfahl, S., Sodemann, H., Eugster, W., and Wernli, H.: Isotope meteorology of cold front passages: A case study combining observations and modelling, Geophys. Res. Lett., 42, 5652–5660, https://doi.org/10.1002/2015GL063988, 2015.

Alexandre, A., Landais, A., Vallet-Coulomb, C., Piel, C., Devidal, S., Pauchet, S., Sonzogni, C., Couapel, M., Pasturel, M., Cornuault, P., Xin, J., Mazur, J. C., Prié, F., Bentaleb, I., Webb, E., Chalié, F., and Roy, J.: The triple oxygen isotope composition of phytoliths as a proxy of continental atmospheric humidity: Insights from climate chamber and climate transect calibrations, Biogeosciences, 15, 3223–3241, https://doi.org/10.5194/bg-15-3223-2018, 2018.

Alexandre, A., Webb, E., Landais, A., Piel, C., Devidal, S., Sonzogni, C., Couapel, M., Mazur, J., Pierre, M., Prié, F., Vallet-Coulomb, C., Outrequin, C., and Roy, J.: Effects of leaf length and development stage on the triple oxygen isotope signature of grass leaf water and phytoliths: insights for a proxy of continental atmospheric humidity, Biogeosciences, 16, 4613–4625, https://doi.org/10.5194/bg-16-4613-2019, 2019.

Arellano, L. N., Beverly, E. J., Voarintsoa, N. R. G., Skinner, C. B., Schauer, A. J., and Steig, E. J.: Triple oxygen isotope variability of precipitation in a tropical mountainous region, Geochim. Cosmochim. Acta, 385, 1–15, https://doi.org/10.1016/j.gca.2024.09.024, 2024.

Arnault, J., Jung, G., Haese, B., Fersch, B., Rummler, T., Wei, J., Zhang, Z., and Kunstmann, H.: A Joint Soil-Vegetation-Atmospheric Modeling Procedure of Water Isotopologues: Implementation and Application to Different Climate Zones With WRF-Hydro-Iso, J. Adv. Model. Eart Syst., 13, e2021MS002562, https://doi.org/10.1029/2021MS002562, 2021.

https://doi.org/10.5194/egusphere-2025-5879
Preprint. Discussion started: 5 December 2025

Aron, P. G., Levin, N. E., Beverly, E. J., Huth, T. E., Passey, B. H., Pelletier, E. M., Poulsen, C. J., Winkelstern, I. Z., and Yarian, D. A.: Triple oxygen isotopes in the water cycle, Chem. Geol., 565, 120026, https://doi.org/10.1016/j.chemgeo.2020.120026, 2021.

Barkan, E., and Luz, B.: High precision measurements of $^{17}O/^{16}O$ and $^{18}O/^{16}O$ ratios in H_2O, Rapid Commun. Mass Spectrom., 19, 3737–3742, https://doi.org/10.1002/rcm.2250, 2005.

Bartsch, S., Stegehuis, A. I., Boissard, C., Lathière, J., Peterschmitt, J. Y., Reiter, I. M., Gauquelin, T., Baldy, V., Genesio, L., Matteucci, G., Fernandez, C., and Guenet, B.: Impact of precipitation, air temperature and abiotic emissions on gross primary production in Mediterranean ecosystems in Europe, Eur. J. For. Res., 139, 111–126, https://doi.org/10.1007/s10342-019-01246-7, 2020.

Bastrikov, V., Steen-Larsen, H. C., Masson-Delmotte, V., Gribanov, K., Cattani, O., Jouzel, J., and Zakharov, V.: Continuous measurements of atmospheric water vapour isotopes in western Siberia (Kourovka), Atmos. Meas. Tech., 7, 1763–1776, https://doi.org/10.5194/amt-7-1763-2014, 2014.

Berkelhammer, M., Hu, J., Bailey, A., Noone, D., Still, C. J., Barnard, H., Gochis, D., Hsiao, G. S., Rahn, T., and Turnipseed, A.: The nocturnal water cycle in an open-canopy forest, J. Geophys. Res. Atmos., 118, 10225–10242, https://doi.org/10.1002/jgrd.50701, 2013.

Bershaw, J., Penny, S. M., and Garzione, C. N.: Stable isotopes of modern water across the Himalaya and eastern Tibetan Plateau: Implications for estimates of paleoelevation and paleoclimate, J. Geophys. Res. Atmos., 117, 1-18, https://doi.org/10.1029/2011JD016132, 2012.

Bland, J. M., and Altman, D. G.: Multiple significance tests: the Bonferroni method. Br. Med. J., 310, 170. https://doi.org/10.1136/bmj.310.6973.170, 1995.

Casellas, E., Latron, J., Cayuela, C., Bech, J., Udina, M., Sola, Y., Lee, K. O., and Llorens, P.: Moisture origin and characteristics of the isotopic signature of rainfall in a Mediterranean mountain catchment (Vallcebre, eastern Pyrenees), J. Hydrol., 575, 767–779, https://doi.org/10.1016/j.jhydrol.2019.05.060, 2019.

Cassou, C.: Intraseasonal interaction between the Madden-Julian Oscillation and the North Atlantic Oscillation, Nature, 455, 523–527, https://doi.org/10.1038/nature07286, 2008.

Cassou, C., Hurrell, J. W., and Deser, C.: North Atlantic Winter Climate Regimes: Spatial Asymmetry, Stationarity with Time, and Oceanic Forcing, J. Clim., 17, 1055–1068, https://doi.org/10.1175/1520-0442(2004)017<1055:NAWCRS>2.0.CO;2, 2004.

Cassou, C., Terray, L., and Phillips, A. S.: Tropical Atlantic Influence on European Heat Waves, J. Clim., 18, 2805–2811, https://doi.org/10.1175/JCLI3506.1, 2005.

Celle-Jeanton, H., Travi, Y., and Blavoux, B.: Isotopic typology of the precipitation in the Western Mediterranean region at the three different time scales, Geophys. Res. Lett., 28, 1215–1218, https://doi.org/10.1029/2000GL012407, 2001.

https://doi.org/10.5194/egusphere-2025-5879
Preprint. Discussion started: 5 December 2025

Craig, H., and Gordon, L. I.: Deuterium and oxygen 18 variations in the ocean and the marine atmosphere, in: Stable Isotopes in Oceanographic Studies and Paleotemperatures, edited by: E. Tongiorgi, Consiglio Nazionale delle Ricerche Laboratorio du Geologia Nucleare, Pisa, Italy, 9–130, http://yncenter.sites.yale.edu/sites/default/files/shen_jing_jan_2013.pdf, 1965.

Cruz-San Julian, J., Araguas-Araguas, L., Rozanski, K., Benavente, J., Cardenal, J., Hidalgo, M. C., Garcia-Lopez, S., Martinez-Garrido, J. C., Moral, F., and Olias, M.: Sources of precipitation over South-Eastern Spain and groundwater recharge. An isotopic study, Tellus B, 44, 226–236, https://doi.org/10.1034/j.1600-0889.1992.t01-2-00005.x, 1992.

Dansgaard, W: Stable isotopes in precipitation, Tellus, 16, 436–468, https://doi.org/10.3402/tellusa.v16i4.8993, 1964.

Delattre, H., Vallet-Coulomb, C., and Sonzogni, C.: Deuterium excess in the atmospheric water vapour of a Mediterranean coastal wetland: regional vs. local signatures, Atmos. Chem. Phys., 15, 10167–10181, https://doi.org/10.5194/acp-15-10167-2015, 2015.

Galewsky, J., Steen-Larsen, H. C., Field, R. D., Worden, J., Risi, C., and Schneider, M.: Stable isotopes in atmospheric water vapor and applications to the hydrologic cycle, Rev. Geophys., 54, 809–865, https://doi.org/10.1002/2015RG000512, 2016.

Gat, J. R.: Oxygen and Hydrogen Isotopes in the Hydrologic Cycle, Annu. Rev. Earth Planet. Sci., 24, 225–262, https://doi.org/10.1146/annurev.earth.24.1.225, 1996.

Gázquez, F., Jiménez-Espejo, F., Rodríguez-Rodríguez, M., Martegani, L., Voigt, C., Ruíz-Lara, D., Moreno, A., Valero-Garcés, B., Morellón, M., and Martín-Puertas, C.: Roman water management impacted the hydrological functioning of wetlands during drought periods, Sci. Rep., 13, 18815, https://doi.org/10.1038/s41598-023-46010-5, 2023.

Gázquez, F., Morellón, M., Bauska, T., Herwartz, D., Surma, J., Moreno, A., Staubwasser, M., Valero-Garcés, B., Delgado-Huertas, A., and Hodell, D. A.: Triple oxygen and hydrogen isotopes of gypsum hydration water for quantitative paleo-humidity reconstruction, Earth Planet. Sci. Lett., 481, 177–188, https://doi.org/10.1016/j.epsl.2017.10.020, 2018.

Giménez, R., Bartolomé, M., Gázquez, F., Iglesias, M., and Moreno, A.: Underlying Climate Controls in Triple Oxygen (^{16}O, ^{17}O, ^{18}O) and Hydrogen (^{1}H, ^{2}H) Isotopes Composition of Rainfall (Central Pyrenees), Front. Earth Sci., 9, 633698, https://doi.org/10.3389/feart.2021.633698, 2021.

Graf, P., Wernli, H., Pfahl, S., and Sodemann, H.: A new interpretative framework for below-cloud effects on stable water isotopes in vapour and rain, Atmos. Chem. Phys., 19, 747–765, https://doi.org/10.5194/acp-19-747-2019, 2019.

Gröning, M., Lutz, H. O., Roller-Lutz, Z., Kralik, M., Gourcy, L., and Pöltenstein, L.: A simple rain collector preventing water re-evaporation dedicated for $\delta^{18}O$ and $\delta^{2}H$ analysis of cumulative precipitation samples, J. Hydrol., 448–449, 195–200, https://doi.org/10.1016/j.jhydrol.2012.04.041, 2012.

Guo, J., Zhang, J., Chen, T., Bai, K., Shao, J., Sun, Y., Li, N., Wu, J., Li, R., Li, J., Guo, Q., Cohen, J. B., Zhai, P., Xu, X., and Hu, F.: A merged continental planetary boundary layer height dataset based on high-resolution radiosonde measurements, ERA5 reanalysis, and GLDAS, Earth Syst. Sci. Data, 16, 1-14, https://doi.org/10.5194/essd-2022-150, 2022.

He, H., & Smith, R. B.: Stable isotope composition of water vapor in the atmospheric boundary layer above the forests of New England, J. Geophys. Res. Atmos., 104, 11657–11673, https://doi.org/10.1029/1999JD900080, 1999.

https://doi.org/10.5194/egusphere-2025-5879
Preprint. Discussion started: 5 December 2025

He, S., Jackisch, D., Samanta, D., Yi, P. K. Y., Liu, G., Wang, X., and Goodkin, N. F.: Understanding Tropical Convection Through Triple Oxygen Isotopes of Precipitation From the Maritime Continent, J. Geophys. Res. Atmos., 126, e2020JD033418, https://doi.org/10.1029/2020JD033418, 2021.

Hersbach, H., Bell, B., Berrisford, P., Hirahara, S., Horányi, A., Muñoz-Sabater, J., Nicolas, J., Peubey, C., Radu, R., Schepers, D., Simmons, A., Soci, C., Abdalla, S., Abellan, X., Balsamo, G., Bechtold, P., Biavati, G., Bidlot, J., Bonavita, M., … Thépaut, J. N.: The ERA5 global reanalysis, Q. J. R. Meteorol. Soc., 146, 1999–2049, https://doi.org/10.1002/qj.3803, 2020.

Huang, L., and Wen, X.: Temporal variations of atmospheric water vapor δD and $\delta^{18}O$ above an arid artificial oasis cropland in the Heihe River Basin, J. Geophys. Res. Atmos., 119, 11456–11476, https://doi.org/10.1002/2014JD021891, 2014.

IAEA/WMO: The Global Network of Isotopes in Precipitation database, https://www.iaea.org/services/networks/gnip, last access: 26 November 2025.

Koren, G., Schneider, L., van der Velde, I. R., van Schaik, E., Gromov, S. S., Adnew, G. A., Mrozek Martino, D. J., Hofmann, M. E. G., Liang, M. C., Mahata, S., Bergamaschi, P., van der Laan-Luijkx, I. T., Krol, M. C., Röckmann, T., and Peters, W.: Global 3-D Simulations of the Triple Oxygen Isotope Signature $\Delta^{17}O$ in Atmospheric CO_2, J. Geophys. Res. Atmos., 124, 8808–8836, https://doi.org/10.1029/2019JD030387, 2019.

Lai, C. T., and Ehleringer, J. R.: Deuterium excess reveals diurnal sources of water vapor in forest air, Oecologia, 165, 213–223, https://doi.org/10.1007/s00442-010-1721-2, 2011.

Landais, A., Barkan, E., and Luz, B.: Record of $\delta^{18}O$ and ^{17}O-excess in ice from Vostok Antarctica during the last 150,000 years, Geophys. Res. Lett., 35, 1–5, https://doi.org/10.1029/2007GL032096, 2008.

Landais, A., Barkan, E., Yakir, D., and Luz, B.: The triple isotopic composition of oxygen in leaf water, Geochim. Cosmochim. Acta, 70, 4105–4115, https://doi.org/10.1016/j.gca.2006.06.1545, 2006.

Landais, A., Risi, C., Bony, S., Vimeux, F., Descroix, L., Falourd, S., and Bouygues, A.: Combined measurements of $^{17}O_{excess}$ and d-excess in African monsoon precipitation: Implications for evaluating convective parameterizations, Earth Planet. Sci. Lett., 298, 104–112, https://doi.org/10.1016/j.epsl.2010.07.033, 2010.

Landais, A., Steen-Larsen, H. C., Guillevic, M., Masson-Delmotte, V., Vinther, B., and Winkler, R.: Triple isotopic composition of oxygen in surface snow and water vapor at NEEM (Greenland), Geochim. Cosmochim. Acta, 77, 304–316, https://doi.org/10.1016/j.gca.2011.11.022, 2012.

Li, S., Levin, N. E., Soderberg, K., Dennis, K. J., and Caylor, K. K.: Triple oxygen isotope composition of leaf waters in Mpala, central Kenya, Earth Planet. Sci. Lett., 468, 38–50, https://doi.org/10.1016/j.epsl.2017.02.015, 2017.

Liang, Q. S., Sha, L. J., Li, J. Y., Zhang, J., Wang, X. J., Zhou, S. L., Lin, F. Y., Xue, Y. X., Duan, R., He, Y. T., Li, H. Y., Wang, C. Y., Liu, B., Hou, Y. K., Chen, C. J., Cheng, H., and Li, T. Y.: Seasonal Variations and Controls on Triple Oxygen and Hydrogen Isotopes in Precipitation—A Case Study From Monitoring in Southwest China, J. Geophys. Res. Atmos., 129, e2023JD040654, https://doi.org/10.1029/2023JD040654, 2024.

https://doi.org/10.5194/egusphere-2025-5879
Preprint. Discussion started: 5 December 2025

Lin, Y., Clayton, R. N., Huang, L., Nakamura, N., and Lyons, J. R.: Oxygen isotope anomaly observed in water vapor from Alert, Canada and the implication for the stratosphere, Proc. Natl. Acad. Sci. U.S.A., 110, 15608–15613, https://doi.org/10.1073/pnas.1313014110, 2013.

Lin, Y., Wu, N., Ta, K., Landais, A., and Peng, X.: Triple Oxygen Isotopic Compositions of Ocean Water from the Mariana Trench, ACS Earth Space Chem., 5, 3087–3096, https://doi.org/10.1021/acsearthspacechem.1c00187, 2021.

Luz, B., and Barkan, E.: Variations of $^{17}O/^{16}O$ and $^{18}O/^{16}O$ in meteoric waters, Geochim. Cosmochim. Acta, 74, 6276–6286, https://doi.org/10.1016/j.gca.2010.08.016, 2010.

Majoube, M.: Fractionnement en oxygène 18 et en deutérium entre l'eau et sa vapeur, J. Chim. Phys., 68, 1423–1436, https://doi.org/10.1051/jcp/1971681423, 1971.

Mercer, J. J., Liefert, D. T., and Williams, D. G.: Atmospheric vapour and precipitation are not in isotopic equilibrium in a continental mountain environment, Hydrol. Process., 34, 3078–3101, https://doi.org/10.1002/hyp.13775, 2020.

Merlivat, L., and Jouzel, J.: Global climatic interpretation of the deuterium-oxygen 18 relationship for precipitation, J. Geophys. Res., 84, 5029–5033, https://doi.org/10.1029/JC084iC08p05029, 1979.

Michelangeli, P.-A., Vautard, R., and Legras, B.: Weather regimes: Recurrence and Quasi Stationarity. J. Atmos. Sci., 52, 1237–1256, https://doi.org/10.1175/1520-0469(1995)052%3C1237:WRRAQS%3E2.0.CO;2, 1995.

Natali, S., Baneschi, I., Doveri, M., Giannecchini, R., Selmo, E., and Zanchetta, G.: Meteorological and geographical control on stable isotopic signature of precipitation in a western Mediterranean area (Tuscany, Italy): Disentangling a complex signal, J. Hydrol., 603, 126944, https://doi.org/10.1016/j.jhydrol.2021.126944, 2021.

Obermann, A., Bastin, S., Belamari, S., Conte, D., Gaertner, M. A., Li, L., and Ahrens, B.: Mistral and Tramontane wind speed and wind direction patterns in regional climate simulations, Clim. Dyn., 51, 1059–1076, https://doi.org/10.1007/s00382-016-3053-3, 2018.

Outrequin, C., Alexandre, A., Vallet-Coulomb, C., Piel, C., Devidal, S., Landais, A., Couapel, M., Mazur, J., Peugeot, C., Pierre, M., Prié, F., Roy, J., Sonzogni, C., and Voigt, C.: The triple oxygen isotope composition of phytoliths, a new proxy of atmospheric relative humidity: controls of soil water isotope composition, temperature, CO_2 concentration and relative humidity, Clim. Past, 17, 1881–1902, https://doi.org/10.5194/cp-17-1881-2021, 2021.

Penchenat, T., Vimeux, F., Daux, V., Cattani, O., Viale, M., Villalba, R., Srur, A., and Outrequin, C.: Isotopic Equilibrium Between Precipitation and Water Vapor in Northern Patagonia and Its Consequences on $\delta^{18}O_{cellulose}$ Estimate, J. Geophys. Res. Biogeosci., 125, e2019JG005418, https://doi.org/10.1029/2019JG005418, 2020.

Pfahl, S., and Wernli, H.: Air parcel trajectory analysis of stable isotopes in water vapor in the eastern Mediterranean, J. Geophys. Res. Atmos., 113, 1–16, https://doi.org/10.1029/2008JD009839, 2008.

Pierchala, A., Rozanski, K., Dulinski, M., and Gorczyca, Z.: Triple-isotope mass balance of mid-latitude, groundwater controlled lake, Sci. Total Environ., 814, 151935, https://doi.org/10.1016/j.scitotenv.2021.151935, 2021.

https://doi.org/10.5194/egusphere-2025-5879
Preprint. Discussion started: 5 December 2025

Ranjan, S., Ramanathan, A. L., Keesari, T., Singh, V. B., Kumar, N., Pandey, M., and Leuenberger, M. C.: Triple Water Vapour–Isotopologues Record from Chhota Shigri, Western Himalaya, India: A Unified Interpretation based on $\delta^{17}O$, $\delta^{18}O$, δD and Comparison to Meteorological Parameters, Front. Earth Sci., 8, 1–16, https://doi.org/10.3389/feart.2020.599632, 2021.

Reiter, I. M., Castagnoli, G., and Rotereau, A.: COOPERATE database [dataset]. https://cooperate.eccorev.fr/db, 2015.

Rothfuss, Y., Quade, M., Brüggemann, N., Graf, A., and Vereecken, H.: Reviews and syntheses: Gaining insights into evapotranspiration partitioning with novel isotopic monitoring methods, Biogeosciences, 18, 3701–3732, https://doi.org/10.5194/bg-18-3701-2021, 2021.

Rozanski, K., Araguás-Araguás, L., and Gonfiantini, R.: Isotopic Patterns in Modern Global Precipitation, in: Climate Change in Continental Isotopic Records, edited by: Swart, K., Lohmann, K.C., Mckenzie, J. and Savin, S., 78, 1–36, https://doi.org/10.1029/gm078p0001, 1993.

Saighi, O.: Isotopic composition of precipitation from Algiers and Assekrem, in: Isotopic composition of precipitation in the Mediterranean Basin in relation to air circulation patterns and climate: final report of a coordinated research project, 2000-2004, edited by: International Atomic Energy Agency, Vienna, Austria, 5–17, ISBN 92–0–105305–3, 2005.

Salmon, O., Welp, L. R., Baldwin, M., Hajny, K., Stirm, B., and Shepson, P.: Vertical profile observations of water vapor deuterium excess in the lower troposphere, Atmos. Chem. Phys., 19, 11525–11543, https://doi.org/10.5194/acp-19-11525-2019, 2019.

Sharp, Z. D., Wostbrock, J. A. G., and Pack, A.: Mass-dependent triple oxygen isotope variations in terrestrial materials, Geochem. Perspect. Lett., 7, 27–31, https://doi.org/10.7185/geochemlet.1815, 2018.

Simonin, K. A., Link, P., Rempe, D., Miller, S., Oshun, J., Bode, C., Dietrich, W. E., Fung, I., and Dawson, T. E.: Vegetation induced changes in the stable isotope composition of near surface humidity, Ecohydrology, 7, 936–949, https://doi.org/10.1002/eco.1420, 2014.

Sodemann, H., Schwierz, C., and Wernli, H.: Interannual variability of Greenland winter precipitation sources: Lagrangian moisture diagnostic and North Atlantic Oscillation influence, J. Geophys. Res. Atmos., 113, 1–17, https://doi.org/10.1029/2007JD008503, 2008.

Sodemann, H., Aemisegger, F., Pfahl, S., Bitter, M., Corsmeier, U., Feuerle, T., Graf, P., Hankers, R., Hsiao, G., Schulz, H., Wieser, A., and Wernli, H.: The stable isotopic composition of water vapour above Corsica during the HyMeX SOP1 campaign: Insight into vertical mixing processes from lower-tropospheric survey flights, Atmos. Chem.Phys., 17, 6125–6151, https://doi.org/10.5194/acp-17-6125-2017, 2017.

Stein, A. F., Draxler, R. R., Rolph, G. D., Stunder, B. J. B., Cohen, M. D., and Ngan, F.: NOAA's HYSPLIT atmospheric transport and dispersion modeling system, Bull. Am. Meteorol. Soc., 96, 2059–2077, https://doi.org/10.1175/BAMS-D-14-00110.1, 2015.

Surma, J., Assonov, S., Bolourchi, M. J., and Staubwasser, M.: Triple oxygen isotope signatures in evaporated water bodies from the Sistan Oasis, Iran, Geophys. Res. Lett., 42, 8456–8462, https://doi.org/10.1002/2015GL066475, 2015.

Surma, J., Assonov, S., Herwartz, D., Voigt, C., and Staubwasser, M.: The evolution of ^{17}O-excess in surface water of the arid environment during recharge and evaporation, Sci. Rep., 8, 1–10, https://doi.org/10.1038/s41598-018-23151-6, 2018.

Surma, J., Assonov, S., and Staubwasser, M.: Triple Oxygen Isotope Systematics in the Hydrologic Cycle, Rev. Mineral. Geochem., 86, 401–428, https://doi.org/10.2138/rmg.2021.86.12, 2021.

Tada, M., Yoshimura, K., and Toride, K.: Improving weather forecasting by assimilation of water vapor isotopes, Sci. Rep., 11, 18067, https://doi.org/10.1038/s41598-021-97476-0, 2021.

Terzer-Wassmuth, S., Araguás-Araguás, L. J., Wassenaar, L. I., and Stumpp, C.: Global and local meteoric water lines for $\delta^{17}O/\delta^{18}O$ and the spatiotemporal distribution of $\Delta'^{17}O$ in Earth's precipitation, Sci. Rep., 13, 19056, https://doi.org/10.1038/s41598-023-45920-8, 2023.

Uemura, R., Barkan, E., Abe, O., and Luz, B.: Triple isotope composition of oxygen in atmospheric water vapor, Geophys. Res. Lett., 37, 1–4, https://doi.org/10.1029/2009GL041960, 2010.

Vallet-Coulomb, C., Couapel, M., and Sonzogni, C.: Improving memory effect correction to achieve high precision analysis of $\delta^{17}O$, $\delta^{18}O$ $\delta^{2}H$, ^{17}O-excess and d-excess in water using cavity ring-down laser spectroscopy, Rapid Commun. Mass Spectrom., 35, e9108, https://doi.org/10.1002/rcm.9108, 2021.

Vautard, R.: Multiple weather regimes over the North Atlantic: Analysis of Precursors and Successors, Mon. Weather Rev., 118, 2056–2081, https://doi.org/10.1175/1520-0493(1990)118%3C2056:MWROTN%3E2.0.CO;2, 1990.

Voarintsoa, N. R. G.: A 3.5-year rainfall isotope records from northwestern Madagascar featuring $^{17}O_{excess}$ and implication for paleoclimate research, Appl. Geochem., 184, 106335, https://doi.org/10.1016/j.apgeochem.2025.106335, 2025.

Voigt, C., Alexandre, A., Reiter, I. M., Orts, J. P., Vallet-Coulomb, C., Piel, C., Mazur, J. C., Aleman, J. C., Sonzogni, C., Miche, H., and Ogée, J.: Examination of the parameters controlling the triple oxygen isotope composition of grass leaf water and phytoliths at a Mediterranean site: a model-data approach, Biogeosciences, 20, 2161–2187, https://doi.org/10.5194/bg-20-2161-2023, 2023.

Voigt, C., Gázquez, F., Martegani, L., Sánchez Villanueva, A. I., Medina, A., Jiménez-Espinosa, R., Jiménez-Millán, J., and Rodríguez-Rodríguez, M.: How seasonal hydroclimate variability drives the triple oxygen and hydrogen isotope composition of small lake systems in semiarid environments, Hydrol. Earth Syst. Sci., 29, 1783-1806, https://doi.org/10.5194/hess-29-1783-2025, 2025.

Voigt, C., Herwartz, D., Dorador, C., and Staubwasser, M.: Triple oxygen isotope systematics of evaporation and mixing processes in a dynamic desert lake system, Hydrol. Earth Syst. Sci., 25, 1211–1228, https://doi.org/10.5194/hess-25-1211-2021, 2021.

waterisotopes-CISE-LOCEAN: Water isotopes of sea water analyzed since 1998 at LOCEAN, SEANOE [dataset], https://doi.org/https://doi.org/10.17882/71186, 2025.

Welp, L. R., Lee, X., Griffis, T. J., Wen, X. F., Xiao, W., Li, S., Sun, X., Hu, Z., Val Martin, M., and Huang, J.: A meta-analysis of water vapor deuterium-excess in the midlatitude atmospheric surface layer, Global Biogeochem. Cycles, 26, 1–12, https://doi.org/10.1029/2011GB004246, 2012.

https://doi.org/10.5194/egusphere-2025-5879
Preprint. Discussion started: 5 December 2025

Xia, Z., Surma, J., and Winnick, M. J.: The response and sensitivity of deuterium and ^{17}O-excess parameters in precipitation to hydroclimate processes, Earth-Sci. Rev., 242, 104432, https://doi.org/10.1016/j.earscirev.2023.104432, 2023.

Xia, Z., Welker, J. M., and Winnick, M. J.: The Seasonality of Deuterium Excess in Non-Polar Precipitation, Global Biogeochem. Cycles, 36, e2021GB007245, https://doi.org/10.1029/2021GB007245, 2022.

Zhang, Y., Legrande, A. N., Goodkin, N., Nusbaumer, J., He, S., Schmidt, G. A., and Wang, X.: Exploring Precipitation Triple Oxygen Isotope Dynamics: Insights from GISS-E2.1 Simulations, J. Adv. Model. Earth Syst., 17, e2024MS004509, https://doi.org/10.1029/2024MS004509, 2025.

Zhao, L., Wang, L., Liu, X., Xiao, H., Ruan, Y., & Zhou, M.: The patterns and implications of diurnal variations in the d-excess of plant water, shallow soil water and air moisture, Hydrol. Earth Syst. Sci., 18, 4129–4151, https://doi.org/10.5194/hess-18-4129-2014, 2014.